Available online at www.sciencedirect.com
SCIENCE DIRECT®
Journal of Sound and Vibration 271 (2004) 815–847
JOURNAL OF SOUND AND VIBRATION
www.elsevier.com/locate/jsvi

Green's matrix and the boundary integral equation method for the analysis of vibration and energy flow in cylindrical shells with and without internal fluid loading

S.V. Sorokin, J.B. Nielsen, N. Olhoff*

Institute of Mechanical Engineering, Aalborg University, Pontoppidanstraede 101, DK 9220, Aalborg, Denmark

Received 9 September 2002; accepted 3 March 2003

Abstract

This paper presents several aspects of the dynamics of a cylindrical shell with and without heavy internal fluid loading, which have not been studied before in detail. Firstly, a consistent formulation of boundary integral equations for a shell of finite length is derived based on the energy conservation principle and the reciprocity theorem. This derivation naturally leads to identification of principal components of the energy flux through an arbitrary cross-section of a shell and to formulation of Green's matrix for an infinitely long shell at each individual circumferential wave number. Secondly, an inspection into the energy re-distribution between several transmission paths in a near field (in a boundary layer at the vicinity of a loaded cross-section) is performed, which sheds light on the role of evanescent waves in motions of a driven shell. Thirdly, the influence of excitation conditions on steady fluctuations of the overall energy flow between transmission paths in a far field is explored for the case, when several propagating waves exist in a shell both with and without internal fluid loading. Besides, a systematic verification of the solution offered by the boundary equations method is given through comparison of eigenfrequencies with those computed in finite element modelling for various boundary conditions. Analysis of dispersion curves and input mobilities is also presented.

1. Introduction

Vibrations of thin walled structures are, in numerous industrial applications, accompanied by sound emission into an acoustic medium. In some cases the 'feedback' influence produced by an acoustic medium on structural vibrations is negligible and the vibro-acoustic behaviour of the structure is entirely defined by the structural properties, e.g., density, Young's modulus, thickness,

*Corresponding author. Tel.: +45-96-35-93-13; fax: +45-98-15-1675.
E-mail address: no@ime.auc.dk (N. Olhoff).

0022-460X/$ - see front matter © 2003 Elsevier Ltd. All rights reserved.
doi:10.1016/S0022-460X(03)00755-7

etc. However there are very many industrial applications where a strong coupling between the structural vibrations and the acoustic field exists—where the 'feedback' of the fluid needs to be considered in the vibro-acoustic analysis [1]. In these cases, simultaneous solution of the coupled equations of dynamics of the structure and the acoustic medium is needed. Apart from this phenomenological classification of problems in dynamics of thin-walled structures into 'light' and 'heavy' fluid loading cases, another classification is alternatively suggested depending on whether a modal approach or a wave approach is applied [2]. In the first case a standing wave solution is sought and in the second a travelling wave solution. The latter may especially be useful if the system has remote parts and the forcing is concentrated in a local area.

In practical engineering design, the finite element method is often regarded as a universal tool for calculations of eigenfrequency spectra, mode shapes and forced vibrations. However it has limitations for unbounded structures and requires very fine meshing when dealing with high frequencies. Although power flow may be obtained from post-processing of the discretised velocities, forces and stresses, it may be difficult to obtain adequate insight into the underlying mechanisms. To obtain fundamental insight into the key transport mechanism and the governing parameters for power flow, analytically based tools may be advantageous.

Such an alternative may be the boundary integral equations method. The method is equally applicable to describe travelling waves in infinite structures and standing waves in finite structures—with and without heavy fluid loading [3–6]. The essence of this method is the use of Green's matrices to formulate the response of a system to a 'fundamental' set of 'basic loading cases' [3]. Then it does not make any difference whether a problem for a finite structure or for an infinite structure is posed. Moreover, from the viewpoint of efficiency of computations, it does not present difficulties to consider a complex structure composed by the 'elementary' segments, provided that their Green's matrices are available. This means the method may be used in a sub-structuring approach.

The boundary integral equations method has been successfully applied for solving various coupled problems in structural acoustics, e.g., in Refs. [4–6]. In particular, this method is suitable and convenient for analysis of dynamics of cylindrical shells, which are widely used in technical applications as elements of many structures, e.g., pipelines, aircraft fuselages, ship hulls, etc. The determination of the dynamic properties of cylindrical shells is thus an important subject in the area of noise and vibration control. Both the modal and the wave problem formulations may be posed for the 'empty' (or 'light' fluid loaded) structure, as well as for the fluid filled (or 'heavy' fluid-loaded) structure. In this paper, Green's matrix and boundary equations are presented in a simple analytical form for a cylindrical shell both with and without an internal fluid loading and a wide range of problems in dynamics of cylindrical shells is solved by use of these tools.

Addressing the existing literature on the subject, two groups of papers should be mentioned. The first one includes papers dealing with analysis of dispersion of linear waves and power flow in infinitely long cylindrical shells with and without fluid loading [7–15]. In particular, the detailed analysis of solution of a homogeneous problem given in Ref. [10] is extended in Refs. [11–13] to calculations of an input mobility and the energy flow in a farfield zone. The results obtained in these papers give a deep insight into the structure of free waves existing in a cylindrical shell with and without fluid loading. An important issue of comparison of the energy distribution between a structure and an acoustic medium in a far field is also carefully studied in these references. As is shown in Ref. [11], in the case of mechanical excitation of a dominantly longitudinal wave in a

fluid-loaded shell, a considerable part of energy may be conveyed to a far field by an acoustic wave. Similar analysis has been recently carried out in Ref. [7] with use of different tools. Ref. [7] also contains a comprehensive list of recent publications on this subject.

Another group of papers is related to use of a boundary equations method in analysis of vibrations of cylindrical shells and in analysis of power flow in beam structures. Refs. [8,16] deal with mobility functions for a cylindrical shell without fluid loading and the concept explored there is fairly close to the contents of earlier papers [3,4]. In Ref. [3], boundary integral equations for vibrations of a cylindrical shell in vacuum have been derived and solutions of several model problems for multi-segment cylindrical shells have been presented. Boundary integral equations are applied to solve coupled problems in structural acoustics in Ref. [4]. Most recently, a concept of boundary integral equations has been used in Refs. [6,9] for analysis and optimisation of power flows in tubular structures and in sandwich plates.

It appears that no publications are available which deal with the formulation and consistent application of Green's matrix and boundary integral equations for analysis of the propagation of waves in cylindrical shells with/without fluid loading and their free/forced vibrations. In particular, a detailed inspection into the energy redistribution between longitudinal, torsional, flexural and acoustic waves in the near field (in the boundary layer located nearby the loaded cross-section of a shell) has not yet been performed. Such an inspection is very important for exploring possibilities of isolation and suppression of vibrations by mechanical dampers mounted at the surface of a shell. Besides, the systematic comparison of eigenfrequencies of cylindrical shells of finite length calculated by the boundary equations method and by the finite element method also presents the aspect of novelty.

The paper is structured as follows. In Section 2, a reciprocity theorem is formulated for a thin elastic cylindrical shell within the framework of general Novozhilov shell theory. Somigliana's identity and a system of boundary integral equations are derived in Section 3 for a shell with no fluid loading. Section 4 contains derivation of components of Green's matrix in such a case. In Section 5, a dependence of purely real, purely imaginary and complex roots of the dispersion equation on an excitation frequency is studied and the shape of Green's functions (a forced response of an infinitely long shell in 'fundamental' loading cases) is analysed. A boundary integral equations method is applied in Section 6 to compute natural frequencies of several cylindrical shells and their magnitudes are verified by comparison with the results obtained by use of a commercial finite element programme. In Section 7, an investigation is carried out into the energy flows in a cylindrical shell with no fluid loading, with emphasis put on energy exchanges between flexural, torsional and longitudinal waves in a near field, e.g., in vicinity of a loaded cross-section. Section 8 contains formulation of Green's matrix for a fluid-loaded shell. In Section 9, dispersion curves for a fluid-loaded shell are analysed and some examples of the shape of Green's functions are given. Finally analysis of the energy transmission in a fluid-loaded shell is performed in Section 10. Most of the attention is focused on the re-distribution of the energy input between flexural, torsional, longitudinal and acoustic waves in various excitation conditions. The mechanism of such a re-distribution is identified and the comparison of the energy flows in a shell without fluid loading and in the fluid-loaded shell is performed. Although the theory outlined in the present paper is easily adjusted for a detailed analysis of frequency spectra in multi-segment shells of a finite length as well as for energy flow calculations for infinitely long multi-segment shells, vibrations of these structures are not tackled in the present paper.

2. Reciprocity theorem

The dynamics of thin cylindrical shells may be described within the framework of various shell theories, e.g., suggested by Flugge, Donnell–Mushtary, Novozhilov–Gol'denveiser, etc., see Ref. [17]. The validity ranges of these theories have been thoroughly studied in numerous publications (see, for example, Refs. [17,18]) and it is not the goal of the present paper to discuss this subject any further. We just note that as is proven in Ref. [18], the asymptotically consistent theory of thin shells based on Kirchhoff–Love hypotheses is the one suggested by Novozhilov and Gol'denveiser [18,19]. Of course, to analyse propagation of comparatively short waves in a cylindrical shell, Timoshenko–Reissner-type theories should be used. However, our analysis is restricted to a frequency range where the characteristic wavelength is markedly larger than the thickness of the shell and Novozhilov–Gol'denveiser theory is adopted hereafter.

A shell of constant thickness h and mid-surface radius R is considered in co-ordinates (x, θ). The Lame parameters and curvatures are, respectively, $A_1 = 1$, $A_2 = R$, $1/R_1 = 0$, $1/R_2 = 1/R$, see Refs. [18,19]. The sign convention adopted in the theory is illustrated in the appendix. To derive boundary equations and a Somigliana identity for a cylindrical shell it is necessary to formulate a reciprocity theorem. This derivation is reproduced here in detail for the stationary case, when time-dependence for all generalised displacements and forces is introduced as $\exp(-i\omega t)$ and this multiplier is omitted.

Two loading cases of a cylindrical shell are considered, which are generated by arbitrary sets of driving forces presented as series of trigonometric functions in the circumferential co-ordinate:

$$q_1(x,\theta) = \sum_m q_{1m}(x)\cos(m\theta),$$
$$q_2(x,\theta) = \sum_m q_{2m}(x)\sin(m\theta),$$
$$q_3(x,\theta) = \sum_m q_{3m}(x)\cos(m\theta) \tag{1a}$$

and

$$q_1^0(x,\theta) = \sum_m q_{1m}^0(x)\cos(m\theta),$$
$$q_2^0(x,\theta) = \sum_m q_{2m}^0(x)\sin(m\theta),$$
$$q_3^0(x,\theta) = \sum_m q_{3m}^0(x)\cos(m\theta). \tag{1b}$$

Here, the origin of the circumferential co-ordinate is chosen arbitrarily. The amplitudes of displacements in these loading cases are expanded in similar series:

$$u(x,\theta) = \sum_m u_m(x)\cos(m\theta),$$
$$v(x,\theta) = \sum_m v_m(x)\sin(m\theta),$$
$$w(x,\theta) = \sum_m w_m(x)\cos(m\theta) \tag{2a}$$

and

$$u^0(x,\theta)=\sum_m u_m^0(x)\cos(m\theta),$$
$$v^0(x,\theta)=\sum_m v_m^0(x)\sin(m\theta),$$
$$w^0(x,\theta)=\sum_m w_m^0(x)\cos(m\theta). \tag{2b}$$

The amplitudes of displacements, deformations, force and moment resultants in the 'trial' state are distinguished from those in the 'actual' state by a superscript 0. To be able to treat an arbitrary loading case, complementary sets of driving loads and displacements where trigonometric functions change places should also be considered. However, due to the periodicity of trigonometric functions, the boundary equations for the two cases are exactly the same.

The reciprocity theorem, which follows from the variational principle is formulated as [18]

$$\begin{aligned}&\int_0^{2\pi}\int_l [T_1\varepsilon_1^0+T_2\varepsilon_2^0+S\varpi^0+M_1\kappa_1^0+M_2\kappa_2^0+2H\tau^0\\&\quad-\rho h\omega^2 uu^0-\rho h\omega^2 vv^0-\rho h\omega^2 ww^0]R\,\mathrm{d}x\,\mathrm{d}\theta\\&\quad=\int_0^{2\pi}\int_l [T_1^0\varepsilon_1+T_2^0\varepsilon_2+S^0\varpi+M_1^0\kappa_1+M_2^0\kappa_2+2H^0\tau\\&\qquad-\rho h\omega^2 u^0u-\rho h\omega^2 v^0v-\rho h\omega^2 w^0w]R\,\mathrm{d}x\,\mathrm{d}\theta.\end{aligned} \tag{3}$$

This formulation differs from its counterpart in statics [19] only by the presence of inertial terms, which apparently are self-balanced. The explicit formulation of deformations, force and moment resultants are given in the appendix. Their substitution into the reciprocity formulation after integration by parts and some simple transformations gives

$$\begin{aligned}&\left[\frac{\mathrm{d}u_m}{\mathrm{d}x}+\frac{m\nu}{R}v_m+\frac{\nu}{R}w_m\right]u_m^0\Big|_{x=0}^{x=l}\\&\quad+\left[-\frac{1-\nu}{2}\frac{m}{R}u_m+\frac{1-\nu}{2}\frac{\mathrm{d}v_m}{\mathrm{d}x}+\frac{h^2}{12}\frac{2(1-\nu)}{R^2}\frac{\mathrm{d}v_m}{\mathrm{d}x}+\frac{h^2}{12}\frac{2(1-\nu)m}{R^2}\frac{\mathrm{d}w_m}{\mathrm{d}x}\right]v_m^0\Big|_{x=0}^{x=l}\\&\quad+\frac{h^2}{12}\left[\frac{\mathrm{d}^2w_m}{\mathrm{d}x^2}-\frac{m^2\nu}{R^2}w_m^0-\frac{m\nu}{R^2}v_m\right]\frac{\mathrm{d}w_m^0}{\mathrm{d}x}\Big|_{x=0}^{x=l}\\&\quad+\frac{h^2}{12}\left[-\frac{\mathrm{d}^3w_m}{\mathrm{d}x^3}+\frac{(2-\nu)m^2}{R^2}\frac{\mathrm{d}w_m}{\mathrm{d}x}+\frac{(2-\nu)m}{R^2}\frac{\mathrm{d}v_m}{\mathrm{d}x}\right]w_m^0\Big|_{x=0}^{x=l}\\&\quad+\int_0^l\left\{\left[-\frac{\mathrm{d}^2u_m}{\mathrm{d}x^2}+\frac{1-\nu}{2}\frac{m^2}{R^2}u_m-\frac{1+\nu}{2}\frac{m}{R}\frac{\mathrm{d}v_m}{\mathrm{d}x}-\frac{\nu}{R}\frac{\mathrm{d}w_m}{\mathrm{d}x}-\frac{\rho\omega^2(1-\nu^2)}{E}u_m\right]u_m^0\right.\\&\quad+\left[\frac{1+\nu}{2}\frac{m}{R}\frac{\mathrm{d}u_m}{\mathrm{d}x}-\frac{1-\nu}{2}\frac{\mathrm{d}^2v_m}{\mathrm{d}x^2}+\frac{m^2}{R^2}v_m-\frac{h^2}{12}\frac{2(1-\nu)}{R^2}\frac{\mathrm{d}^2v_m}{\mathrm{d}x^2}+\frac{h^2}{12}\frac{m^2}{R^4}v_m\right.\end{aligned}$$

$$
\begin{aligned}
&+\frac{m}{R^2}w_m+\frac{h^2}{12}\frac{m^3}{R^4}w_m-\frac{h^2}{12}\frac{(2-\nu)m}{R^2}\frac{\mathrm{d}^2w_m}{\mathrm{d}x^2}-\frac{\rho\omega^2(1-\nu^2)}{E}v_m\Big]v_m^0\\
&+\Big[\frac{\nu}{R}\frac{\mathrm{d}u_m}{\mathrm{d}x}+\frac{m}{R^2}v_m+\frac{h^2}{12}\frac{m^3}{R^4}v_m-\frac{h^2}{12}\frac{(2-\nu)m}{R^2}\frac{\mathrm{d}^2v_m}{\mathrm{d}x^2}+\frac{1}{R^2}w_m+\frac{h^2}{12}\frac{\mathrm{d}^4w_m}{\mathrm{d}x^4}\\
&-\frac{h^2}{12}\frac{2m^2}{R^2}\frac{\mathrm{d}^2w_m}{\mathrm{d}x^2}+\frac{h^2}{12}\frac{m^4}{R^4}w_m-\frac{\rho\omega^2(1-\nu^2)}{E}w_m\Big]w_m^0\Big\}\,\mathrm{d}x
\end{aligned}
$$

$$
\begin{aligned}
=&\left[\frac{\mathrm{d}u_m^0}{\mathrm{d}x}+\frac{m\nu}{R}v_m^0+\frac{\nu}{R}w_m^0\right]u_m\Big|_{x=0}^{x=l}\\
&+\left[-\frac{1-\nu}{2}\frac{m}{R}u_m^0+\frac{1-\nu}{2}\frac{\mathrm{d}v_m^0}{\mathrm{d}x}+\frac{h^2}{12}\frac{2(1-\nu)}{R^2}\frac{\mathrm{d}v_m^0}{\mathrm{d}x}+\frac{h^2}{12}\frac{2(1-\nu)m}{R^2}\frac{\mathrm{d}w_m^0}{\mathrm{d}x}\right]v_m\Big|_{x=0}^{x=l}\\
&+\frac{h^2}{12}\left[\frac{\mathrm{d}^2w_m^0}{\mathrm{d}x^2}-\frac{m^2\nu}{R^2}w_m^0-\frac{m\nu}{R^2}v_m^0\right]\frac{\mathrm{d}w_m}{\mathrm{d}x}\Big|_{x=0}^{x=l}\\
&+\frac{h^2}{12}\left[-\frac{\mathrm{d}^3w_m^0}{\mathrm{d}x^3}+\frac{(2-\nu)m^2}{R^2}\frac{\mathrm{d}w_m^0}{\mathrm{d}x}+\frac{(2-\nu)m}{R^2}\frac{\mathrm{d}v_m^0}{\mathrm{d}x}\right]w_m\Big|_{x=0}^{x=l}\\
&+\int_0^l\Big\{\left[-\frac{\mathrm{d}^2u_m^0}{\mathrm{d}x^2}+\frac{1-\nu}{2}\frac{m^2}{R^2}u_m^0-\frac{1+\nu}{2}\frac{m}{R}\frac{\mathrm{d}v_m^0}{\mathrm{d}x}-\frac{\nu}{R}\frac{\mathrm{d}w_m^0}{\mathrm{d}x}-\frac{\rho\omega^2(1-\nu^2)}{E}u_m^0\right]u_m\\
&+\Big[\frac{1+\nu}{2}\frac{m}{R}\frac{\mathrm{d}u_m^0}{\mathrm{d}x}-\frac{1-\nu}{2}\frac{\mathrm{d}^2v_m^0}{\mathrm{d}x^2}+\frac{m^2}{R^2}v_m^0-\frac{h^2}{12}\frac{2(1-\nu)}{R^2}\frac{\mathrm{d}^2v_m^0}{\mathrm{d}x^2}+\frac{h^2}{12}\frac{m^2}{R^4}v_m^0\\
&+\frac{m}{R^2}w_m^0+\frac{h^2}{12}\frac{m^3}{R^4}w_m^0-\frac{h^2}{12}\frac{(2-\nu)m}{R^2}\frac{\mathrm{d}^2w_m^0}{\mathrm{d}x^2}-\frac{\rho\omega^2(1-\nu^2)}{E}v_m^0\Big]v_m\\
&+\Big[\frac{\nu}{R}\frac{\mathrm{d}u_m^0}{\mathrm{d}x}+\frac{m}{R^2}v_m^0+\frac{h^2}{12}\frac{m^3}{R^4}v_m^0-\frac{h^2}{12}\frac{(2-\nu)m}{R^2}\frac{\mathrm{d}^2v_m^0}{\mathrm{d}x^2}+\frac{1}{R^2}w_m^0+\frac{h^2}{12}\frac{\mathrm{d}^4w_m^0}{\mathrm{d}x^4}\\
&-\frac{h^2}{12}\frac{2m^2}{R^2}\frac{\mathrm{d}^2w_m^0}{\mathrm{d}x^2}+\frac{h^2}{12}\frac{m^4}{R^4}w_m^0-\frac{\rho\omega^2(1-\nu^2)}{E}w_m^0\Big]w_m\Big\}\,\mathrm{d}x. \qquad (4)
\end{aligned}
$$

The expressions in curly brackets are in fact the differential operators of equations of stationary forced vibrations of a cylindrical shell, i.e., the set of ordinary differential equations in terms of the unknown modal amplitudes (u_m, v_m, w_m) is obtained:

$$
-\frac{\mathrm{d}^2u_m}{\mathrm{d}x^2}+\frac{1-\nu}{2}\frac{m^2}{R^2}u_m-\frac{1+\nu}{2}\frac{m}{R}\frac{\mathrm{d}v_m}{\mathrm{d}x}-\frac{\nu}{R}\frac{\mathrm{d}w_m}{\mathrm{d}x}-\frac{\rho\omega^2(1-\nu^2)}{E}u_m=q_{1m}\frac{(1-\nu^2)}{Eh}, \qquad (5a)
$$

$$
\begin{aligned}
&\frac{1+\nu}{2}\frac{m}{R}\frac{\mathrm{d}u_m}{\mathrm{d}x}-\frac{1-\nu}{2}\frac{\mathrm{d}^2v_m}{\mathrm{d}x^2}+\frac{m^2}{R^2}v_m-\frac{h^2}{12}\frac{2(1-\nu)}{R^2}\frac{\mathrm{d}^2v_m}{\mathrm{d}x^2}+\frac{h^2}{12}\frac{m^2}{R^4}v_m\\
&+\frac{m}{R^2}w_m+\frac{h^2}{12}\frac{m^3}{R^4}w_m-\frac{h^2}{12}\frac{(2-\nu)m}{R^2}\frac{\mathrm{d}^2w_m}{\mathrm{d}x^2}-\frac{\rho\omega^2(1-\nu^2)}{E}v_m=q_{2m}\frac{(1-\nu^2)}{Eh}, \qquad (5b)
\end{aligned}
$$

$$\frac{v}{R}\frac{\mathrm{d}u_m}{\mathrm{d}x}+\frac{m}{R^2}v_m+\frac{h^2}{12}\frac{m^3}{R^4}v_m-\frac{h^2}{12}\frac{(2-v)m}{R^2}\frac{\mathrm{d}^2v_m}{\mathrm{d}x^2}+\frac{1}{R^2}w_m+\frac{h^2}{12}\frac{\mathrm{d}^4w_m}{\mathrm{d}x^4}$$
$$-\frac{h^2}{12}\frac{2m^2}{R^2}\frac{\mathrm{d}^2w_m}{\mathrm{d}x^2}+\frac{h^2}{12}\frac{m^4}{R^4}w_m-\frac{\rho\omega^2(1-v^2)}{E}w_m=q_{3m}\frac{(1-v^2)}{Eh}. \tag{5c}$$

These equations are derived for an arbitrary loading of the shell and they are equally valid for any number of circumferential waves m. In some references, the 'bending' terms

$$\frac{h^2}{12}\frac{m^3}{R^4}w_m-\frac{h^2}{12}\frac{(2-v)m}{R^2}\frac{\mathrm{d}^2w_m}{\mathrm{d}x^2}$$

in the second equation and

$$\frac{h^2}{12}\frac{m^3}{R^4}v_m-\frac{h^2}{12}\frac{(2-v)m}{R^2}\frac{\mathrm{d}^2v_m}{\mathrm{d}x^2}$$

in the third one are omitted, and this may result in significant errors in describing vibrations at all numbers m, see Refs. [18,19]. The two other 'bending' terms in the second equation,

$$-\frac{h^2}{12}\frac{2(1-v)}{R^2}\frac{\mathrm{d}^2v_m}{\mathrm{d}x^2}+\frac{h^2}{12}\frac{m^2}{R^4}v_m,$$

are also omitted in many references. Although their contribution is negligibly small in most of the cases, it becomes essential for flexural vibrations ($m=1$) of a long shell (see Ref. [18]).

Non-integral terms in Eq. (4) formulate couples of generalised displacements and generalised forces, which are involved in the boundary conditions. It is convenient to introduce the following notations for generalised forces:

$$Q_{1m}=\frac{\mathrm{d}u_m}{\mathrm{d}x}+\frac{mv}{R}v_m+\frac{v}{R}w_m, \tag{6a}$$

$$Q_{2m}=-\frac{1-v}{2}\frac{m}{R}u_m+\frac{1-v}{2}\frac{\mathrm{d}v_m}{\mathrm{d}x}+\frac{h^2}{12}\frac{2(1-v)}{R^2}\frac{\mathrm{d}v_m}{\mathrm{d}x}+\frac{h^2}{12}\frac{2(1-v)m}{R^2}\frac{\mathrm{d}w_m}{\mathrm{d}x}, \tag{6b}$$

$$Q_{3m}=-\frac{h^2}{12}\left[\frac{\mathrm{d}^3w_m}{\mathrm{d}x^3}-\frac{(2-v)m^2}{R^2}\frac{\mathrm{d}w_m}{\mathrm{d}x}-\frac{(2-v)m}{R^2}\frac{\mathrm{d}v_m}{\mathrm{d}x}\right], \tag{6c}$$

$$Q_{4m}=\frac{h^2}{12}\left[\frac{\mathrm{d}^2w_m}{\mathrm{d}x^2}-\frac{m^2v}{R^2}w_m-\frac{mv}{R^2}v_m\right]. \tag{6d}$$

Thus, Eq. (4) formulate the reciprocity theorem for the segment of a cylindrical shell $(0,l)$ in two arbitrary loading cases, which conveniently leads to formulation of Somigliana identities.

3. Somigliana identities

So far no assumptions have been adopted concerning physical meanings of the 'trial' loading case $(q^0_{1m},q^0_{2m},q^0_{3m})$ and the trial solution (u^0_m,v^0_m,w^0_m). Now it is convenient to formulate three sets of functions $(u^{0j}_m(|x-\xi|),v^{0j}_m(|x-\xi|),w^{0j}_m(|x-\xi|))$, $j=1,2,3$ as the amplitudes of vibrations of an infinitely long cylindrical shell loaded by the three sets of driving forces $(\delta(x-\xi),0,0)$,

$(0, \delta(x-\xi), 0)$ and $(0, 0, \delta(x-\xi))$. Then Eq. (4) due to the fundamental property of the delta-function is transformed to three Somigliana identities for each of these loading cases:

$$u_m(\xi) = \left[Q_{1m}(x) u_m^{01}(x,\xi) + Q_{2m}(x) v_m^{01}(x,\xi) + Q_{3m}(x) w_m^{01}(x,\xi) + Q_{4m}(x) \frac{\partial w_m^{01}(x,\xi)}{\partial x} \right] \Big|_{x=0}^{x=l}$$
$$- \left[Q_{1m}^{01}(x,\xi) u_m(x) + Q_{2m}^{01}(x,\xi) v_m(x) + Q_{3m}^{01}(x,\xi) w_m(x) + Q_{4m}^{01}(x,\xi) \frac{\mathrm{d}w_m(x)}{\mathrm{d}x} \right] \Big|_{x=0}^{x=l}$$
$$+ \frac{1-\nu^2}{Eh} \int_0^l [q_{1m}(x) u_m^{01}(x,\xi) + q_{2m}(x) v_m^{01}(x,\xi) + q_{3m}(x) w_m^{01}(x,\xi)] \, \mathrm{d}x, \tag{7a}$$

$$v_m(\xi) = \left[Q_{1m}(x) u_m^{02}(x,\xi) + Q_{2m}(x) v_m^{02}(x,\xi) + Q_{3m}(x) w_m^{02}(x,\xi) + Q_{4m}(x) \frac{\partial w_m^{02}(x,\xi)}{\partial x} \right] \Big|_{x=0}^{x=l}$$
$$- \left[Q_{1m}^{02}(x,\xi) u_m(x) + Q_{2m}^{02}(x,\xi) v_m(x) + Q_{3m}^{02}(x,\xi) w_m(x) + Q_{4m}^{02}(x,\xi) \frac{\mathrm{d}w_m(x)}{\mathrm{d}x} \right] \Big|_{x=0}^{x=l}$$
$$+ \frac{1-\nu^2}{Eh} \int_0^l [q_{1m}(x) u_m^{02}(x,\xi) + q_{2m}(x) v_m^{02}(x,\xi) + q_{3m}(x) w_m^{02}(x,\xi)] \, \mathrm{d}x, \tag{7b}$$

$$w_m(\xi) = \left[Q_{1m}(x) u_m^{03}(x,\xi) + Q_{2m}(x) v_m^{03}(x,\xi) + Q_{3m}(x) w_m^{03}(x,\xi) + Q_{4m}(x) \frac{\partial w_m^{03}(x,\xi)}{\partial x} \right] \Big|_{x=0}^{x=l}$$
$$- \left[Q_{1m}^{03}(x,\xi) u_m(x) + Q_{2m}^{03}(x,\xi) v_m(x) + Q_{3m}^{03}(x,\xi) w_m(x) + Q_{4m}^{03}(x,\xi) \frac{\mathrm{d}w_m(x)}{\mathrm{d}x} \right] \Big|_{x=0}^{x=l}$$
$$+ \frac{1-\nu^2}{Eh} \int_0^l [q_{1m}(x) u_m^{03}(x,\xi) + q_{2m}(x) v_m^{03}(x,\xi) + q_{3m}(x) w_m^{03}(x,\xi)] \, \mathrm{d}x. \tag{7c}$$

Similarly to the case of flexural vibrations of a plate (see Refs. [3,5,6]), an additional identity is formulated with respect to the first derivative of the radial displacement w. It is obtained by differentiation of Eq. (7c) with respect to the co-ordinate ξ of the 'observation point':

$$\frac{\mathrm{d}w_m(\xi)}{\mathrm{d}\xi} = \left[Q_{1m}(x) \frac{\partial u_m^{03}(x,\xi)}{\partial \xi} + Q_{2m}(x) \frac{\partial v_m^{03}(x,\xi)}{\partial \xi} + Q_{3m}(x) \frac{\partial w_m^{03}(x,\xi)}{\partial \xi} + Q_{4m}(x) \frac{\partial^2 w_m^{03}(x,\xi)}{\partial \xi \, \partial x} \right] \Big|_{x=0}^{x=l}$$
$$- \left[\frac{\partial Q_{1m}^{03}(x,\xi)}{\partial \xi} u_m(x) + \frac{\partial Q_{2m}^{03}(x,\xi)}{\partial \xi} v_m(x) + \frac{\partial Q_{3m}^{03}(x,\xi)}{\partial \xi} w_m(x) + \frac{\partial Q_{4m}^{03}(x,\xi)}{\partial \xi} \frac{\mathrm{d}w_m(x)}{\mathrm{d}x} \right] \Big|_{x=0}^{x=l}$$
$$+ \frac{1-\nu^2}{Eh} \int_0^l \left[q_{1m}(x) \frac{\partial u_m^{03}(x,\xi)}{\partial \xi} + q_{2m}(x) \frac{\partial v_m^{03}(x,\xi)}{\partial \xi} + q_{3m}(x) \frac{\partial w_m^{03}(x,\xi)}{\partial \xi} \right] \mathrm{d}x. \tag{7d}$$

The four identities (7) contain 16 unknown values of boundary displacements and generalised forces at the edges of the shell. Respectively, eight boundary equations are obtained by putting an observation point at the edge $x = 0$ and at the edge $x = l$.

For a shell of a finite length, the boundary conditions are formulated at the edges $x = 0$, $x = l$ as

$$\begin{aligned}
&\chi_{11} Q_{1m} + \chi_{12} u_m = 0,\\
&\chi_{21} Q_{2m} + \chi_{22} v_m = 0,\\
&\chi_{31} Q_{3m} + \chi_{32} w_m = 0,\\
&\chi_{41} Q_{4m} + \chi_{42} \frac{\mathrm{d}w_m}{\mathrm{d}x} = 0
\end{aligned} \tag{8a}$$

and

$$\begin{aligned}
&\chi_{51} Q_{1m} + \chi_{52} u_m = 0,\\
&\chi_{61} Q_{2m} + \chi_{62} v_m = 0,\\
&\chi_{71} Q_{3m} + \chi_{72} w_m = 0,\\
&\chi_{81} Q_{4m} + \chi_{82} \frac{\mathrm{d}w_m}{\mathrm{d}x} = 0.
\end{aligned} \tag{8b}$$

An arbitrary set of conditions may be modelled by the appropriate choice of the coefficients χ_{ij}, $i = 1, 2, \ldots, 8$, $j = 1, 2$ (for example, the set $\chi_{i2} = 0$, $i = 1, 2, \ldots, 8$ defines an unconstrained shell). Then a system of algebraic equations (7)–(8) is composed, which uniquely defines the amplitudes of forced vibrations of a cylindrical shell of finite length.

An exact solution to the problem of forced vibrations of a cylindrical shell with arbitrary boundary conditions at arbitrary frequency for arbitrary circumferential wave number is obtained by solving this system. It may also be conveniently used to determine eigenfrequencies of a shell. To use these equations for practical computations, Green's matrix should be set up.

4. Green's matrix

Elements of Green's matrix are introduced as the amplitudes of displacements in the axial, circumferential and radial directions of an infinitely long cylindrical shell vibrating at its mth circumferential mode in response to four fundamental 'loading cases', see Ref. [3]. For example, the elements of the first row of Green's matrix should satisfy a set of ordinary differential equations:

$$-\frac{\partial^2 u_m^{01}}{\partial x^2} + \frac{1-\nu}{2}\frac{m^2}{R^2} u_m^{01} - \frac{1+\nu}{2}\frac{m}{R}\frac{\partial v_m^{01}}{\partial x} - \frac{\nu}{R}\frac{\partial w_m^{01}}{\partial x} - \frac{\rho\omega^2(1-\nu^2)}{E} u_m^{01} = \delta(x-\xi), \tag{9a}$$

$$\begin{aligned}
&\frac{1+\nu}{2}\frac{m}{R}\frac{\partial u_m^{01}}{\partial x} - \frac{1-\nu}{2}\frac{\partial^2 v_m^{01}}{\partial x^2} + \frac{m^2}{R^2} v_m^{01} - \frac{h^2}{12}\frac{2(1-\nu)}{R^2}\frac{\partial^2 v_m^{01}}{\partial x^2} + \frac{h^2}{12}\frac{m^2}{R^4} v_m^{01}\\
&\quad + \frac{m}{R^2} w_m^{01} + \frac{h^2}{12}\frac{m^3}{R^4} w_m^{01} - \frac{h^2}{12}\frac{(2-\nu)m}{R^2}\frac{\partial^2 w_m^{01}}{\partial x^2} - \frac{\rho\omega^2(1-\nu^2)}{E} v_m^{01} = 0,
\end{aligned} \tag{9b}$$

$$\begin{aligned}
&\frac{\nu}{R}\frac{\partial u_m^{01}}{\partial x} + \frac{m}{R^2} v_m^{01} + \frac{h^2}{12}\frac{m^3}{R^4} v_m^{01} - \frac{h^2}{12}\frac{(2-\nu)m}{R^2}\frac{\partial^2 v_m^{01}}{\partial x^2} + \frac{1}{R^2} w_m^{01} + \frac{h^2}{12}\frac{\partial^4 w_m^{01}}{\partial x^4}\\
&\quad - \frac{h^2}{12}\frac{2m^2}{R^2}\frac{\partial^2 w_m^{01}}{\partial x^2} + \frac{h^2}{12}\frac{m^4}{R^4} w_m^{01} - \frac{\rho\omega^2(1-\nu^2)}{E} w_m^{01} = 0.
\end{aligned} \tag{9c}$$

A solution of this system is not uniquely defined unless some additional conditions are formulated, e.g., conditions at infinity. To be more precise, this inhomogeneous system uniquely defines a particular solution, which actually pertains a unit jump in the real part of the axial force at $x=\xi$, see the right hand side of Eq. (9a). Any general solution of the system of homogeneous equations (9) may be added to this particular solution. If the Green's function is formulated for solving problems in dynamics of both the infinitely long shell and the shell of a finite length, then a general solution should be chosen to satisfy the well-known Sommerfeld radiation conditions [1] at infinity and the Green's function is defined uniquely. However, if the Green's function is derived only for the formulation of boundary equations, then the general solution may be chosen arbitrarily. Specifically, as is discussed in Ref. [3], computations are most efficient when the sum of the particular and the general solutions is a real-valued function.

Similarly to the case of a vibrating beam, due to the natural symmetry of an infinitely long cylindrical shell with respect to each cross-section, the elements of Green's matrix may be obtained by solving the problem for a semi-infinite structure, which is extended either at $-\infty<x<\xi$ or at $\xi<x<\infty$. Dynamics of both these parts of a shell is described by a homogeneous set of differential equations (the loading term in Eq. (9a) is omitted) with the following four loading conditions at the cross-section $x=\xi$, see Refs. [3,4]:

$$\begin{aligned}
&Q^{01}_{1m}(x,\xi)=\frac{\partial u^{01}_{1m}(x,\xi)}{\partial x}+\frac{m\nu}{R}v^{01}_{1m}(x,\xi)+\frac{\nu}{R}w^{01}_{1m}(x,\xi)=-\frac{1}{2}\operatorname{sgn}(x-\xi),\\
&v^{01}_{m}(x,\xi)=0,\\
&w^{01}_{m}(x,\xi)=0,\\
&Q^{01}_{4m}(x,\xi)=\frac{h^2}{12}\left[\frac{\partial^2 w^{01}_{m}(x,\xi)}{\partial x^2}-\frac{m^2\nu}{R^2}w^{01}_{m}(x,\xi)-\frac{m\nu}{R^2}v^{01}_{m}(x,\xi)\right]=0.
\end{aligned}\tag{10}$$

The first condition formulates a unit jump in the magnitude of an axial force at $x=\xi$, the remaining homogeneous ones formulate the symmetry of wave propagation in a shell to the left and to the right from the loaded cross-section.

To obtain the solution to such a problem, the roots of the dispersion polynomial of homogeneous equations (9) should be found, as will be discussed in Section 5. Then the first row of Green's matrix is formulated as

$$\begin{aligned}
u^{01}_{m}&=\sum_{j=1}^{4}\alpha_j C^{01}_{j}\exp\left(\frac{\tilde{k}_j}{R}|x-\xi|\right),\\
v^{01}_{m}&=\operatorname{sgn}(x-\xi)\sum_{j=1}^{4}\beta_j C^{01}_{j}\exp\left(\frac{\tilde{k}_j}{R}|x-\xi|\right),\\
w^{01}_{m}&=\operatorname{sgn}(x-\xi)\sum_{j=1}^{4}C^{01}_{j}\exp\left(\frac{\tilde{k}_j}{R}|x-\xi|\right).
\end{aligned}\tag{11}$$

Four coefficients C_j^{01}, $j=1,2,3,4$ are found from the loading conditions (10). It gives the following set of four inhomogeneous algebraic equations:

$$\frac{1}{R}\sum_{j=1}^{4}\alpha_j\tilde{k}_jC_j^{01}=-\frac{1}{2},$$

$$\sum_{j=1}^{4}\beta_jC_j^{01}=0,$$

$$\sum_{j=1}^{4}C_j^{01}=0,$$

$$\sum_{j=1}^{4}\tilde{k}_j^2C_j^{01}=0.$$

The suggested procedure is in effect identical to perform the Fourier transform for solving the inhomogeneous system of equations (9) with Sommerfeld conditions.

Similarly, the second loading case is formulated with respect to a circumferential force $Q_{2m}^{02}(x,\xi)$, which is distributed in the circumferential direction as $\cos m\theta$ and concentrated in the axial direction

$$\begin{aligned}
&u_m^{02}(x,\xi)=0,\\
&Q_{2m}^{02}(x,\xi)=-\frac{1-\nu}{2}\frac{m}{R}u_m^{02}+\frac{1-\nu}{2}\frac{\partial v_m^{02}}{\partial x}+\frac{h^2}{12}\frac{2(1-\nu)}{R^2}\frac{\partial v_m^{02}}{\partial x}+\frac{h^2}{12}\frac{2(1-\nu)m}{R^2}\frac{\partial w_m^{02}}{\partial x}=-\frac{1}{2}\operatorname{sgn}(x-\xi),\\
&Q_{3m}^{02}(x,\xi)=-\frac{h^2}{12}\left[\frac{\partial^3 w_m^{02}}{\partial x^3}-\frac{(2-\nu)m^2}{R^2}\frac{\partial w_m^{02}}{\partial x}-\frac{(2-\nu)m}{R^2}\frac{\partial v_m^{02}}{\partial x}\right]=0,\\
&\frac{\partial w_m^{02}(x,\xi)}{\partial x}=0.
\end{aligned}\tag{12}$$

The relevant system of algebraic equations is formulated as

$$\sum_{j=1}^{4}\alpha_jC_j^{02}=0,$$

$$\frac{1}{R}\sum_{j=1}^{4}\left[\frac{1-\nu}{2}+\frac{h^2}{12}\frac{2(1-\nu)}{R^2}\right]\beta_j\tilde{k}_jC_j^{02}=-\frac{1}{2},$$

$$-\frac{h^2}{12}\sum_{j=1}^{4}[\tilde{k}_j^3-(2-\nu)m\beta_j\tilde{k}_j]C_j^{02}=0,$$

$$\sum_{j=1}^{4}\tilde{k}_jC_j^{02}=0.$$

Finally, the third row of Green's matrix is defined by the following loading case:

$$
\begin{aligned}
&u_m^{03}(x,\xi) = 0,\\
&Q_{2m}^{03}(x,\xi) = -\frac{1-\nu}{2}\frac{m}{R}u_m^{03} + \frac{1-\nu}{2}\frac{\partial v_m^{03}}{\partial x} + \frac{h^2}{12}\frac{2(1-\nu)}{R^2}\frac{\partial v_m^{03}}{\partial x} + \frac{h^2}{12}\frac{2(1-\nu)m}{R^2}\frac{\partial w_m^{03}}{\partial x} = 0,\\
&Q_{3m}^{03}(x,\xi) = -\frac{h^2}{12}\left[\frac{\partial^3 w_m^{03}}{\partial x^3} - \frac{(2-\nu)m^2}{R^2}\frac{\partial w_m^{03}}{\partial x} - \frac{(2-\nu)m}{R^2}\frac{\partial v_m^{03}}{\partial x}\right] = -\frac{1}{2}\operatorname{sgn}(x-\xi),\\
&\frac{\partial w_m^{03}(x,\xi)}{\partial x} = 0.
\end{aligned}
\tag{13}
$$

The system of algebraic equations defining coefficients C_j^{03}, $j = 1,2,3,4$ then becomes

$$
\begin{aligned}
&\sum_{j=1}^{4}\alpha_j C_j^{03} = 0,\\
&\sum_{j=1}^{4}\left[\frac{1-\nu}{2} + \frac{h^2}{12}\frac{2(1-\nu)}{R^2}\right]\beta_j\tilde{k}_j C_j^{03} = 0,\\
&-\frac{h^2}{12R^3}\sum_{j=1}^{4}[\tilde{k}_j^3 - (2-\nu)m\beta_j\tilde{k}_j]C_j^{03} = -\frac{1}{2},\\
&\sum_{j=1}^{4}\tilde{k}_j C_j^{03} = 0.
\end{aligned}
$$

For the second and the third loading cases, skew symmetry is related to the u displacement i.e., $\operatorname{sgn}(x-\xi)$ is introduced in u instead of in v and w as in the first loading case. The fourth loading case is related to vibrations of an infinitely long cylindrical shell excited by a concentrated bending moment. However, the elements of the fourth row in the matrix may also be obtained by differentiation of the elements of the third row on the co-ordinate of an excitation point, see Refs. [3,5,6] and this way is simpler and more convenient.

5. Dispersion curves and modal coefficients

As is shown in the previous section, to construct Green's matrix it is necessary to find the roots of the dispersion polynomial for a set of homogeneous differential equations (9) by the standard substitution

$$
u_m^{0N} = A\exp\left(\frac{\tilde{k}_j}{R}|x-\xi|\right), \quad v_m^{0N} = B\exp\left(\frac{\tilde{k}_j}{R}|x-\xi|\right), \quad w_m^{0N} = C\exp\left(\frac{\tilde{k}_j}{R}|x-\xi|\right). \tag{14}
$$

In these formulas, $N = 1,2,3$ is the number of the loading case. As functions (14) are substituted into the differential equations (9), a homogeneous system of three algebraic equations in A, B, C is obtained. The condition of an existence of a non-trivial solution is formulated by equating the

following determinant to zero:

$$\begin{vmatrix} d_{11} & d_{12} & d_{13} \\ d_{21} & d_{22} & d_{23} \\ d_{31} & d_{32} & d_{33} \end{vmatrix} = 0 \tag{15}$$

with the elements

$$d_{11} = -\tilde{k}^2 + \frac{1-\nu}{2} m^2 - \Omega^2, \quad d_{12} = -\frac{1+\nu}{2} \tilde{k} m = -d_{21}, \quad d_{13} = -\nu \tilde{k} = -d_{31},$$

$$d_{22} = -\frac{1-\nu}{2} \tilde{k}^2 + m^2 - \Omega^2 - \frac{h^2}{12R^2} 2(1-\nu)\tilde{k}^2 + \frac{h^2}{12R^2} m^2,$$

$$d_{23} = m + \frac{h^2}{12R^2} m^3 - \frac{h^2}{12R^2} (2-\nu) m \tilde{k}^2 = d_{32},$$

$$d_{33} = 1 + \frac{h^2}{12R^2} \tilde{k}^4 - \frac{h^2}{12R^2} 2m^2 \tilde{k}^2 + \frac{h^2}{12R^2} m^4 - \Omega^2, \quad \Omega^2 = \frac{\rho \omega^2 (1-\nu^2) R^2}{E}.$$

The dispersion polynomial is of the fourth order in $\tilde{k}^2$ and its roots are found by use of the symbolic manipulator *Maple V*.[1] If the elastic modulus E has an imaginary part describing the effect of material losses, then four roots $k_j, j = 1, 2, 3, 4$ are selected as those having negative real parts to ensure decay of waves at a large distance from the cross-section where a concentrated force is applied. If no material losses are accounted for, then in addition to the roots having negative real part, purely imaginary roots with positive sign are selected. Since time-dependence is chosen as $\exp(-i\omega t)$, such roots describe travelling waves coming from an excitation point to infinity. In all cases, the number of roots retained in the analysis is four. To identify the type of a wave relevant to the particular root, the modal coefficients introduced as

$$\alpha_j = \frac{A_j}{C_j}, \quad \beta_j = \frac{B_j}{C_j}$$

are found by solving the system of equations

$$\begin{aligned} d_{11}\alpha_j + d_{12}\beta_j &= -d_{13}, \\ d_{21}\alpha_j + d_{22}\beta_j &= -d_{23}. \end{aligned} \tag{16}$$

In Fig. 1, the set of dispersion curves is plotted for $R = 20$ mm, $h = 0.35$ mm, $\nu = 0.3$, $E = 210 \times 10^9$ N/m^2, $\rho = 7800$ kg/m^3, $m = 1, 2, 3, 4, 5$. As is seen, the propagation of waves at arbitrary low frequencies is possible only for $m = 1$ (beam-like vibrations). To demonstrate the applicability of Novozhilov–Gol'denveiser theory to describe this type of shell motions, the dispersion curve derived from elementary Kirchhoff beam theory is displayed in thick black for the lower frequency range. For any $m > 1$, wave propagation is possible only when the excitation frequency exceeds its cut-on value. As is seen, the cut-on frequency increases as the circumferential wave number increases. This phenomenon is well known, see for example

[1] Maple V, Waterloo Maple Inc., Waterloo, Canada.

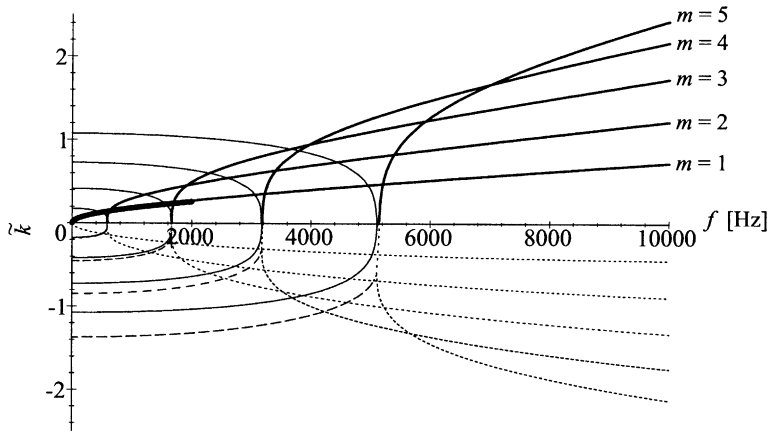

Fig. 1. Dispersion relation for cylindrical shell without fluid, $m = 1$–5: --- Re, comp; — Im, comp; ···· Re, — Im.

Ref. [10]. As discussed, the number of selected roots of the dispersion equation is four, whereas only two dispersion curves are plotted in Fig. 1 for each circumferential wave number. The magnitudes of both the real and the imaginary part of two other roots remain in the range 8.5..11 for $m = 1..5$ and the relevant curves are left out for reasons of clarity.

A closer inspection into the dispersion phenomena involved in generation of a propagating wave is given in Figs. 2 and 3 for $m = 3$. The circumferential mode $m = 3$ is here chosen as a general representative for all shell type motions. Fig. 2 shows the overall behaviour while Fig. 3 zooms in on the first cut-on. It is here noted that the first cut-on takes place just above 1659 Hz as the result of a bifurcation. As is seen, two complex conjugate wave numbers firstly merge and transform into two purely real ones. Then one of these purely real roots continues to grow and transforms to a purely imaginary one as it crosses the axis, whereas the second root decreases. This 'two-phase' transformation occurs in a very narrow frequency band. With further growth in the excitation frequency, two complex conjugate roots transform to two purely evanescent ones, so that in the frequency range from approximately 48.5 to 77 kHz there exist one propagating wave and three evanescent waves. The second propagating wave is generated in a different manner—at $f = 77$ kHz a purely real wave number becomes purely imaginary, thus a decaying wave is converted directly to a propagating wave. Even at this high frequency the wavelengths of the propagating waves are much larger than the thickness of the shell so the shell theory is entirely applicable.

Other valuable information concerning phenomena related to energy input and transportation may be obtained from the modal coefficients. In Fig. 4 the modal coefficients for the waves involved in the first cut-on is displayed—α_3 being linked with the decaying wave and α_4 with the propagating wave. As the two complex conjugate waves merge, their modal coefficients become purely real. At the first cut-on frequency, the modal coefficient of the 'transforming' wave crosses zero and become purely imaginary. Significant changes around this bifurcation and cut-on is only found in α_3 and α_4. All other modal coefficients are stable and almost constant across this frequency range. Thus, at this specific frequency, the longitudinal displacement is uncoupled from the radial and circumferential components of the displacement.

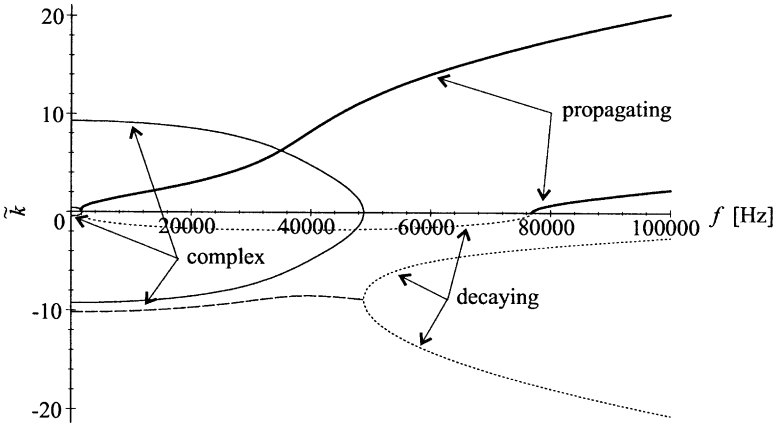

Fig. 2. Dispersion curves for $m = 3$ showing the typical bifurcations: - - - Re, comp; — Im, comp; ···· Re, — Im.

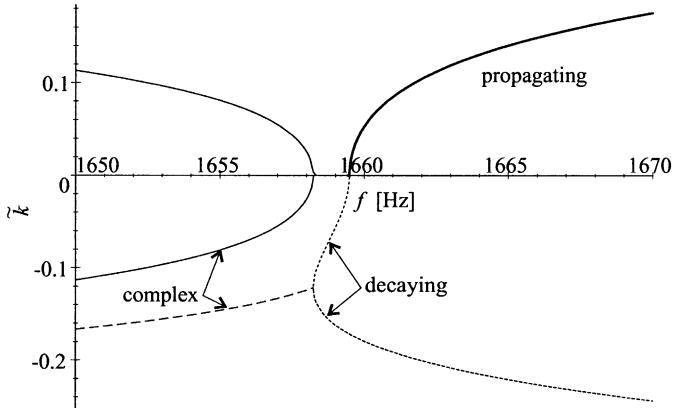

Fig. 3. Zoom on first bifurcation and cut-on for $m = 3$: - - - Re, comp; — Im, comp; ···· Re, — Im.

At higher frequencies during the second bifurcation and cut-on, equivalent changes are seen on several other modal coefficients, some of them shown in Fig. 5. At the bifurcation point of 48.5 kHz the second set of complex conjugates are converted to decaying waves, and $\alpha_1, \beta_1, \alpha_2$ and β_2 turn purely real. At the second cut-on at 77 kHz—related to cut-on of wave no. 3—the modal coefficient turns towards infinity, indicating uncoupled u and w motions of this wave at this specific frequency. Observation on α_4 also reveals a zero-crossing and thus uncoupling within this propagating wave around 32 000 Hz.

The above inspection into the character of wave motions at the cut-on frequencies sheds light on the qualitative difference between admittances of the shell in different excitation conditions. Within the framework of Green's functions concept, admittance is simply the displacement in the direction of excitation at the cross-section of excitation. In Figs. 6 and 7 the input admittance for excitation by longitudinal, circumferential and radial forcing is displayed for $m = 3$. Similar analysis of input admittance for a cylindrical shell at $m = 0$ may be found in Ref. [16]. The total

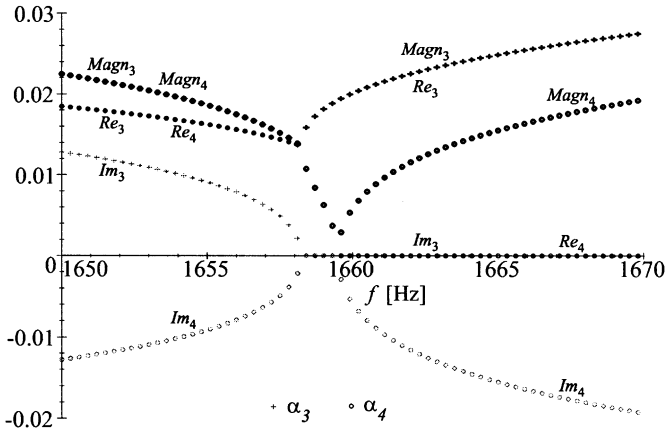

Fig. 4. Zoom on the modal coefficients α_3 and α_4 for $m = 3$ around first bifurcation.

response of the shell is of course related to the magnitude of the admittance. However the injected and transmitted power for a real-valued excitation is only related to the imaginary part of the admittance, i.e.,

- in the case of excitation by an axial force, to: $\mathrm{Im}(u_m^{01}(0,0))$,
- in the case of excitation by a circumferential force, to: $\mathrm{Im}(v_m^{02}(0,0))$,
- in the case of excitation by a radial force, to: $\mathrm{Im}(w_m^{03}(0,0))$,
- in the case of excitation by a moment, to: $\mathrm{Im}(w_m'^{04}(0,0))$.

Below the first cut-on—appearing just below 1660 Hz—no energy may propagate in the shell and the admittance remains purely real. During cut-on a significant difference is seen in the behaviour of the imaginary part of the input admittance for the three loading cases. For the tangential and the radial excitation a very large imaginary part instantly appears, whereas for the longitudinal excitation a gradual increase from the zero value cut-on is observed. This may be explained from the modal coefficients. Here it was observed that α_4 are zero at cut-on—meaning that u is uncoupled from w and thus the u displacement remains bounded while v and w become unbounded. Similar behaviour is observed at second cut-on, just with roles inverted. Here modal coefficient α_3 peaks, indicating that the w motion is uncoupled from the u motion, and as β_3 remains finite this indicates that v is also uncoupled from u. This explains why the admittance from tangential and radial excitation remains bounded while the admittance related to longitudinal excitation peaks towards infinity. So from a vibration-transmission point of view tangential and radial excitation will be critical at frequencies around 1660 Hz whereas longitudinal excitation will not reach its most critical value until around 77 kHz.

Another interesting phenomenon can be observed around 32 kHz. Here a 'dropout'—or an 'anti-resonance'—of the imaginary part of the admittance is found. This corresponds to the second zero-crossing of α_4 in Fig. 4. Thus no energy can be supplied by longitudinal excitation at this frequency. This may also be explained on the level of wave amplitudes. As the calculated wave amplitudes for given excitation appear in complex conjugate pairs for the complex waves and as real for the decaying waves, they solely contribute to the real part of the input admittance. Only

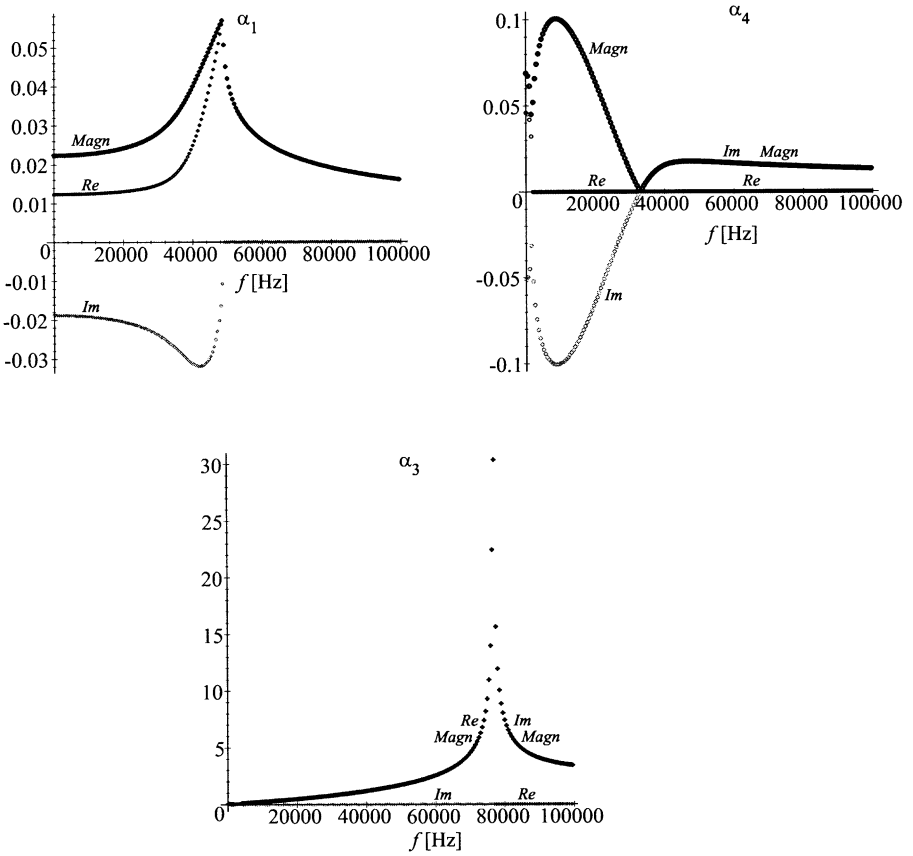

Fig. 5. Modal coefficients α_1, α_3 and α_4 for $m = 3$.

the propagating waves contribute to the imaginary part. This means that if one attempts to excite the structure in a direction that for the propagating wave is uncoupled at the frequency of excitation, no energy is absorbed. There is simply no initial 'link' to the motion that is carrying the energy.

In the admittance only the values of the Green's functions at the point of excitation is considered. However the spatial distribution of the Green's functions—displacement as well as generalised forces—also play an important role. The current Green's functions represent the response to a unit value of $q_m(1-\upsilon^2)/Eh$ and thus allow the generalised force to be interpreted as transfer ratios of the physical forces. The dependence of the modulus, the real and the imaginary parts of the lateral displacement v_3^{03} and the circumferential generalised force Q_{23}^{03} upon axial co-ordinate is presented in Fig. 8 for the case of a radial excitation of the cylindrical shell. Here the amplitude of the circumferential displacement gradually reaches its maximum at $x \approx 0.015$ m. The amplitude of the circumferential force grows very quickly from zero to its maximum value exceeding the magnitude of the input force almost by a factor of 1.5 and then levelling out around 0.8 times the input force. Such a rapid change in the magnitude of a force is typical for several loading conditions.

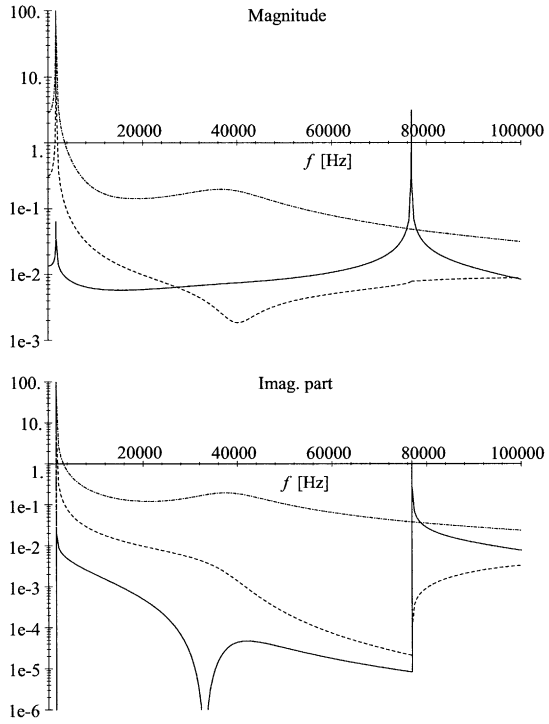

Fig. 6. Input admittance for longitudinal, tangential and radial excitation—magnitude and imaginary part: —— Long exc; – – – – Tang exc; –○–○– Rad. exc.

The forced response of a cylindrical shell to the local driving force described by Green's functions may always be decomposed to the sum of propagating and evanescent waves. The propagating waves constitute the far field of the shell, whereas contribution of the evanescent ones is essential only in the boundary layer near the excitation. However, as will be shown in Section 7, the evanescent waves control the dispersal of the injected power into longitudinal, torsional and flexural components and a rather intense redistribution of energy may take place within this zone. Knowing the detailed behaviour within the near field could thus be beneficial in noise control, as the possibilities to suppress wave motion in this zone may be wider than in the far field.

The axial extension of this boundary is defined by the magnitude of the smallest real part of complex (and real) wave numbers. If considering Fig. 1 it is noted that the purely decaying wave—with a negative real valued wave number—has a order of magnitude that is similar to the propagating wave number except for frequencies very close to cut-on. This means that by moving approximately 0.7 times the farfield wavelength away from the point of excitation, the response attributed to the decaying wave is reduced by a factor of 100. For the complex waves it was noted that the decaying part remained in the range -8.5 to -11, which means the motion related to these wave numbers will be reduced by a factor of 100 within an axial distance of approximately $0.5R$. These considerations may be used for preliminary evaluation of possible spatial extension of the near field and agrees quite well with the behaviour found in Fig. 8.

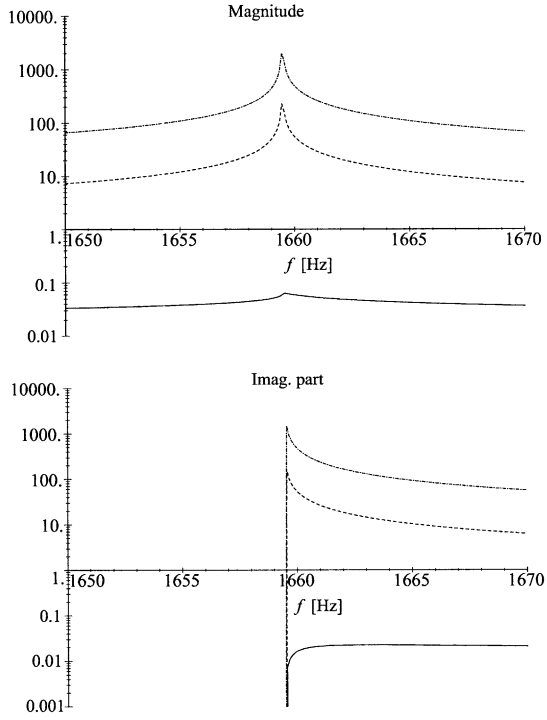

Fig. 7. Zoom on input admittance for longitudinal, tangential and radial excitation—magnitude and imaginary part: —— Long exc; – – – – Tang exc; –○–○– Rad. exc.

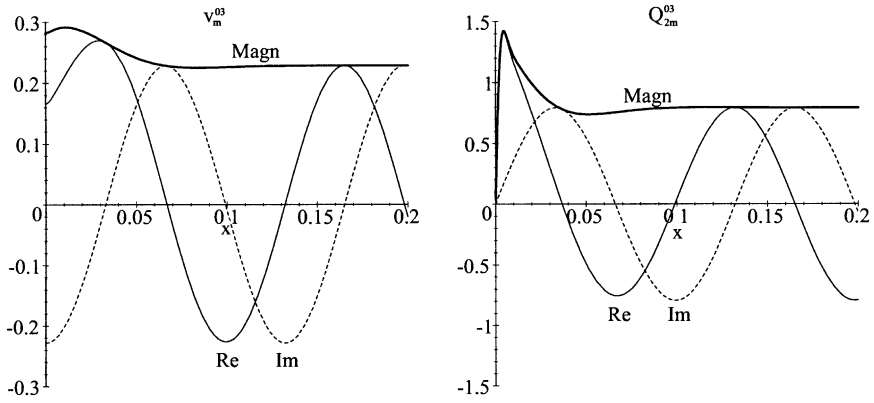

Fig. 8. Examples of Green's functions displaying displacement v_m^{03} and generalised force Q_{2m}^{03} for $m = 3, f = 4000$ Hz.

6. Finite cylindrical shells—verification of boundary equations

The boundary equations for vibrations of a shell of finite length are formulated when the elements of Green's matrix are substituted in Eqs. (7) and an 'observation point' ξ tends to the edge from inside of the shell, i.e., $\xi = 0 + \hat{\varepsilon}$ or $\xi = l - \hat{\varepsilon}$, $\hat{\varepsilon} \to 0$.

Table 1
Comparison of eigenfrequencies from the boundary integral method and the finite element method

Boundary condition	m	n	ANSYS	BIM	Δ (%)
Thin shell geometry					
Clamped–clamped	5	1	9558	9566	0.08
	6	1	10212	10226	0.14
	4	1	10545	10550	0.05
	7	1	12137	12163	0.21
Navier	5	1	7411	7420	0.13
	4	1	7711	7714	0.04
	6	1	8859	8876	0.20
	3	1	10545	10546	0.00
Free–free	2	0	584	583	0.16
	2	1	821	822	0.10
	3	0	1650	1650	0.02
	3	1	2046	2049	0.15
	4	0	3162	3164	0.04
	4	1	3630	3637	0.19
	5	0	5111	5116	0.10
Pipe like geometry					
Clamped–clamped	2	1	5949	5959	0.16
	3	1	10843	10909	0.61
	2	2	11333	11346	0.11
Navier	2	1	4489	4502	0.29
	1	1	6394	6398	0.07
	2	2	9344	9353	0.09
	3	1	10592	10661	0.65
Free–free	2	0	3658	3664	0.16
	2	1	3763	3768	0.14
	2	2	6666	6677	0.16
	3	0	10298	10361	0.61
	3	1	10432	10501	0.66
	3	2	11294	11378	0.74

The test problem of free vibrations of an isolated cylindrical shell under various boundary conditions has been solved to validate the numerical algorithm. The analysis was performed with two different geometries: one thin-walled shell with radius $R = 20$ mm, thickness $h = 0.35$ mm and length $l = 35$ mm and a second 'pipe-like' geometry with $R = 13.5$ mm, thickness $h = 1$ mm and length $l = 100$ mm. Both with material properties $E = 210 \times 10^9$ N/m^2, $\rho = 7800$ kg/m^3 and $\upsilon = 0.3$. In Table 1 the results have then been compared with eigenfrequencies obtained by use of ANSYS finite element software[2] and very satisfactory agreement is found. To be noted is that in

[2] ANSYS Swanson Analysis Systems, Inc., Houston, PA, USA.

the case of Navier boundary conditions $Q_{1m} = v_m = w_m = Q_{4m} = 0$ at the edges $x = 0$ and l, analytical eigenfrequencies of the shell may also be found directly from Eq. (15) if the longitudinal wavenumber is introduced as $k = in\pi R/l$, where n is a positive integer.

7. Power flow

The reciprocity theorem (4) is easily generalised to formulate an energy flow through arbitrary cross-section of a shell at each circumferential number, see Refs. [10–15] for details. It is convenient to present an energy flow at each circumferential wave number as

$$N_{m,out}^{str,tot} = N_{m,out}^{axial} + N_{m,out}^{torsion} + N_{m,out}^{bending}. \tag{17}$$

Here the contributions of longitudinal, torsional and flexural components are presented explicitly:

$$N_{m,out}^{axial} = -\gamma\pi R\frac{\omega}{2}\frac{Eh}{(1-\nu^2)}[\mathrm{Im}(u_m)\cdot\mathrm{Re}(Q_{1m}) - \mathrm{Re}(u_m)\,\mathrm{Im}(Q_{1m})].$$

$$N_{m,out}^{torsion} = -\gamma\pi R\frac{\omega}{2}\frac{Eh}{(1-\nu^2)}[\mathrm{Im}(v_m)\cdot\mathrm{Re}(Q_{2m}) - \mathrm{Re}(v_m)\,\mathrm{Im}(Q_{2m})],$$

$$\begin{aligned} N_{m,out}^{bending} = &-\gamma\pi R\frac{\omega}{2}\frac{Eh}{(1-\nu^2)}[\mathrm{Im}(w_m)\cdot\mathrm{Re}(Q_{3m}) - \mathrm{Re}(w_m)\,\mathrm{Im}(Q_{3m})] \\ &-\gamma\pi R\frac{\omega}{2}\frac{Eh}{(1-\nu^2)}[\mathrm{Im}(w_m')\cdot\mathrm{Re}(Q_{4m}) - \mathrm{Re}(w_m')\,\mathrm{Im}(Q_{4m})], \end{aligned} \tag{18}$$

where $\gamma = 2$ if $m = 0$ and $\gamma = 1$ if $m \neq 0$.

The overall energy flow is obtained by summation of energy flows at different circumferential numbers.

In the literature (see Refs. [10–15] for example), attention has been focused at farfield analysis of the energy flow, whereas in practical applications it is also very important to analyse a nearfield power flow. As discussed in Section 5 the existence of such a near field is actually related to the presence of a boundary layer in the vicinity of the excitation cross-section of the cylindrical shell. Within this boundary layer, the power input produced by driving forces is transmitted to the propagating modes.

Another aspect, which has not yet received attention, is the 'modal' approach to the analysis of energy transportation. Specifically, a power flow in the far field is often calculated simply as a contribution from 'propagating' wave numbers (in our notations, those purely imaginary ones which have positive imaginary parts). However, a shell theory suggests that three different types of waves exist in a cylindrical shell—dominantly flexural, torsional and longitudinal waves. As is seen from Eq. (14), each individual wave number actually contributes to each of these three types of waves, but these contributions are dependent upon excitation conditions and shell parameters. This aspect is very important because devices which suppress propagation of dominantly flexural waves are different from those for suppression of dominantly longitudinal waves and, as is well known [2], it is much easier to suppress flexural vibrations than tangential ones. For this purpose it is, as discussed in Section 5, important to know the length of the boundary layer where possible damping devices may be applied.

In the case of mechanical excitation of wave motions in a shell by a transverse force, the dominantly flexural wave is developed in the boundary layer. However, in parts remote from the excitation point most of energy may be conveyed by longitudinal or torsional waves. Thus analysis of interaction between waves in the nearfield zone becomes of primary interest, as it is in this zone the energy 'injected' into a shell by a transverse driving force is redistributed from flexural waves to tangential ones.

In the following energy transportation in the shell geometry introduced in Section 5 will be studied in detail.

We begin with the case of radial excitation at the frequency $f = 1661$ Hz, which slightly exceeds the first cut-on frequency, i.e., the case when only one wave propagates in the shell. In the left part of Fig. 9 the energy distribution is displayed—with the upper graph zooming in on the intense redistribution in the boundary layer, where the energy injected in radial direction almost immediately is converted into power flow related to tangential motion. Gradually radial motion then regains the energy and in the far field this motion is responsible for approximately 70% of the power flow at this frequency. At a slightly higher frequency $f = 2000$ Hz—displayed in the right part of Fig. 9—similar phenomena with a very rapid exchange just after injection is seen. However at this frequency the radial motion later only regains a very limited amount of energy. In the far field the main power flow is split between longitudinal and tangential motion. To further

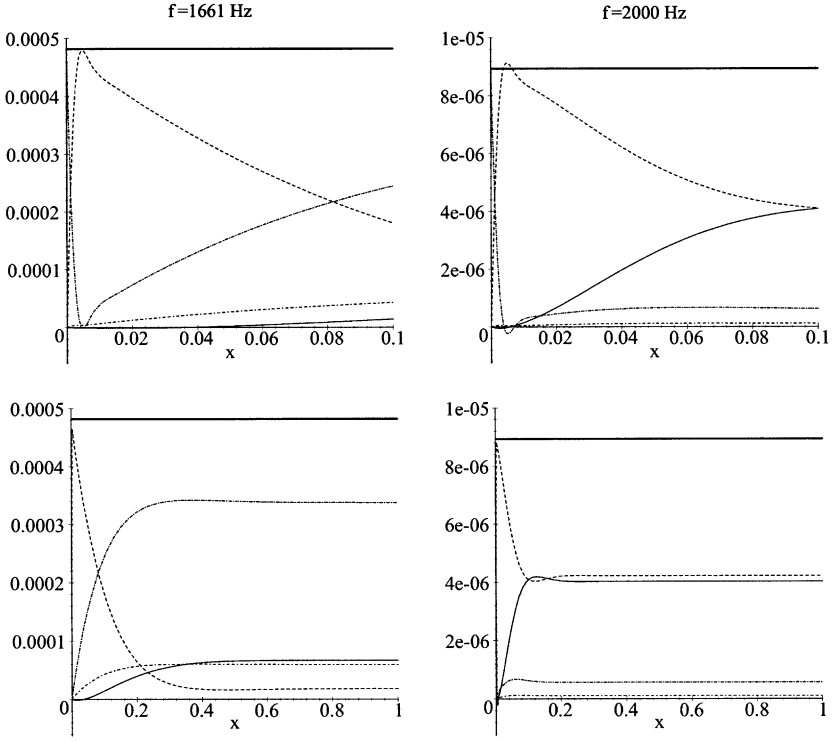

Fig. 9. The power flow balance at frequencies of 1661 and 2000 Hz for $m = 3$: —— N^{axial}; - - - - $N^{torsion}$; —○—○— $N^{bending,w}$; ○○—○○—○○ $N^{bending,w'}$; —— $N^{scr,tot}$.

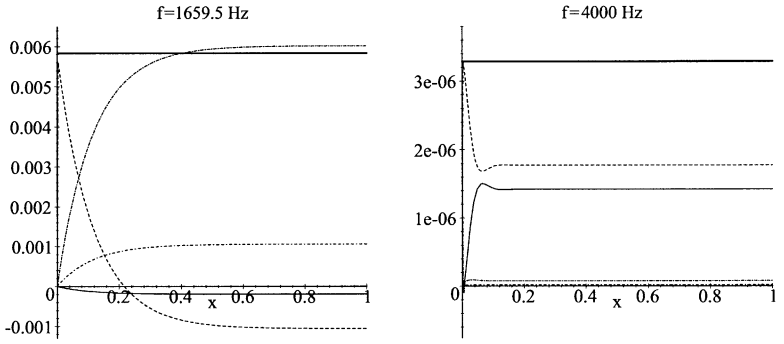

Fig. 10. The power flow balance at frequencies of 1659.5 and 4000 Hz for $m = 3$: —— N^{axial}; ---- $N^{torsion}$; —○—○— $N^{bending,w}$; ○○—○○—○○ $N^{bending,w'}$; —— $N^{scr,tot}$.

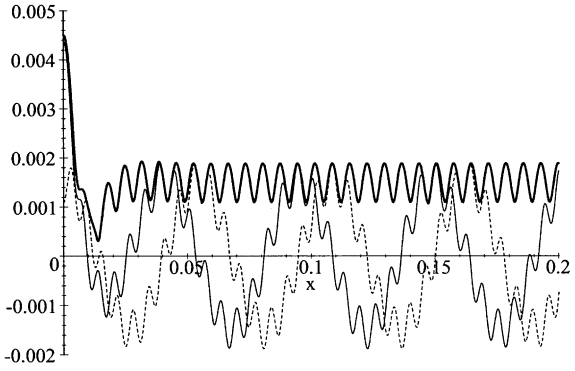

Fig. 11. Green's function v_m^{03} for $m = 3$ at 100 kHz: —— Real; –––– Imag; —— Magn.

illustrate the profound frequency dependence of the energy redistribution, the power flow for $f = 1659.5$ and 4000 Hz is presented in Fig. 10. It is observed that immediately after cut-on the energy flow from radial motion closely resembles the total power flow in the far field and longitudinal and radial motion only account for a small energy flow that is even in reverse direction. As the frequency of excitation is increased, longitudinal and tangential motion gradually takes over the power flow and at 4000 Hz the power flow from radial motion is diminutive in the far field even when the original power is injected purely in that direction.

In the previous case the relative energy distribution in the far field was identical and stable, no matter how the energy was injected. However, at higher frequencies more than one wave may propagate and the cross-coupling between the propagating waves may produce spatial oscillations of displacements, generalised forces and power flow. In Fig. 11 the Green's functions v_m^{03} for an excitation frequency of 100 kHz—where two waves may propagate—is displayed. Just after the second cut-on a very large difference in wavelengths exists between the propagating waves. At 100 kHz there is a ratio of 8.8 between the wavelength of the second cut-on wave and the first cut-on wave—a difference very clearly seen in the figure. The various excitation conditions will excite the two propagating waves differently, which means that the oscillations in the total amplitude will depend upon excitation.

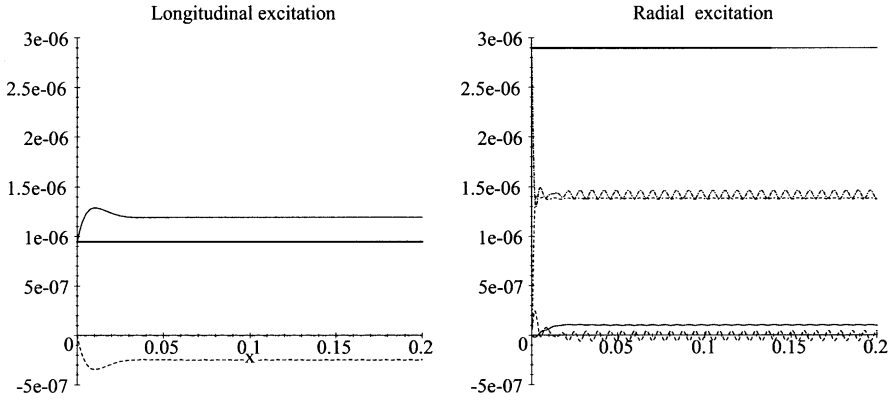

Fig. 12. Power flow for longitudinal and radial excitation at 100 kHz: —— N^{axial}; ---- $N^{torsion}$; —○—○— $N^{bending,w}$; ○○—○○—○○ $N^{bending,w'}$; —— $N^{scr,tot}$.

At 100 kHz the ratio between the excited amplitudes for the first cut-on wave and the second cut-on is 0.13 for longitudinal loading and 35 for radial loading. Thus the final power flow balance depends very much upon type and direction of excitation as seen in Fig. 12. For the longitudinal excitation the dominant carrier of energy is the longitudinal motion with a negative contribution from tangential motion and negligible power flow from radial displacement. For the radial excitation the situation is reversed. The power flow is completely contained within the radial displacements and only tiny amounts of energy are attributed to longitudinal and tangential motion. Due to the very large differences in wave amplitudes the cross-coupling effects and oscillatory content in the power flow is rather limited. However, at even higher frequencies very significant oscillations are found—e.g., at 140 kHz, where peak-to-peak oscillations within one component of power flow may be as large as 80% of the total power flow.

8. Green's matrix—including internal fluid loading

The results reported in the previous sections of the paper are applicable for analysis of wave propagation in cylindrical shells with light fluid loading. However, as it has been discussed in the introduction, it is quite typical in many technical applications to deal with vibrations of e.g., a cylindrical shell filled with some rather dense compressible fluid. In such a case, vibrations of the shell are strongly coupled with the fluid's motions.

The Green's matrix is constructed by solving the shell equations (5) simultaneously with the Helmholtz equation

$$\frac{\partial^2\varphi}{\partial r^2}+\frac{1}{r}\frac{\partial\varphi}{\partial r}-\frac{m^2}{r^2}\varphi+\frac{\partial^2\varphi}{\partial x^2}+\left(\frac{\omega}{c_f}\right)^2\varphi=0, \tag{19}$$

with φ being the acoustic velocity potential.

The fluid–structure interaction is then defined by a continuity condition formulated at the surface of a shell $r = R$ as

$$\frac{\partial \varphi}{\partial r} = -\mathrm{i}\omega w. \tag{20}$$

Eq. (5c) then contains the contact pressure defined by the formula $p = \mathrm{i}\rho_f \omega \varphi$ and may be re-written as

$$\frac{\nu}{R}\frac{\partial u_m}{\partial x} + \frac{m}{R} v_m + \frac{h^2}{12}\frac{m^3}{R^4} v_m - \frac{h^2}{12}\frac{(2-\nu)m}{R^2}\frac{\partial^2 v_m}{\partial x^2} + \frac{1}{R^2} w_m^{01} + \frac{h^2}{12}\frac{\partial^4 w_m}{\partial x^4} - \frac{h^2}{12}\frac{2m^2}{R^2}\frac{\partial^2 w_m}{\partial x^2} + \frac{h^2}{12}\frac{m^4}{R^4} w_m - \frac{\rho\omega^2(1-\nu^2)}{E} w_m - \mathrm{i}\rho_f \omega \frac{1-\nu^2}{Eh}\varphi_m = 0. \tag{21}$$

Displacements are sought in the form (3) and a general solution of Eq. (19) is

$$\varphi(x, r, \theta) = D_m \mathrm{I}_m(\kappa r) \exp\left(\frac{\tilde{k}}{R} x\right) \cos m\theta, \quad \kappa^2 = -\left(\frac{\tilde{k}}{R}\right)^2 - \left(\frac{\omega}{c_f}\right)^2.$$

The 'fluid' modal coefficient is found from the condition

$$D_m \left.\frac{\mathrm{d}\mathrm{I}_m(\kappa r)}{\mathrm{d}r}\right|_{r=R} = -\mathrm{i}\omega C_m.$$

Then the fluid loading term in Eq. (21) becomes

$$-\rho_f \omega^2 \frac{(1-\nu^2)}{Eh} \mathrm{I}_m(\kappa R)\left(\left.\frac{\mathrm{d}\mathrm{I}_m(\kappa r)}{\mathrm{d}r}\right|_{r=R}\right)^{-1}.$$

The dispersion equation (15) is composed of the same elements as for an 'empty' shell, but the last one is modified as

$$d_{33} = 1 + \frac{h^2}{12R^2}\tilde{k}^4 - \frac{h^2}{12R^2} 2m^2\tilde{k}^2 + \frac{h^2}{12R^2} m^4 - \Omega^2 - \rho_f \omega^2 R^2 \frac{(1-\nu^2)}{Eh} \times \mathrm{I}_m(\kappa R)\left(\left.\frac{\mathrm{d}\mathrm{I}_m(\kappa r)}{\mathrm{d}r}\right|_{r=R}\right)^{-1}.$$

The properties of the roots of the dispersion relation are studied most carefully in Refs. [10,12,13]. For example, in Ref. [10], it has been found that the dispersion equation has an infinitely large number of roots and the vast majority of these roots are related to evanescent 'fluid-dominated' waves. However, since the attention in these references has been focused on the energy transmission in a far field, the role of evanescent waves in the boundary layer in the fluid-filled shell near the excitation point has not been studied in detail.

In the present case, similarly to the case of an empty shell, Green's matrix is obtained in the form of expansion of the coupled response of a shell and a fluid on all normal modes, which exist in this system. Thus, it is necessary to retain evanescent modes together with propagating ones. Although these evanescent waves do not transport energy, they control the input mobility of a fluid-loaded shell. Similarly to the case of a shell without fluid loading, these waves act in the boundary layer as 'transducers' of the energy of vibrations from the directly excited waves to the propagating ones.

As has been discussed in Section 1, the standard technique to formulate the stationary forced response of a fluid-filled cylindrical shell is Fourier transformation. Then the amplitudes of radial displacements and all other physical variables are available in the integral form. In computations of these integrals in a complex plane, contribution of a finite number of poles is taken, see Refs. [10–15]. Although the methodology we use here (which has been suggested in Ref. [6]) is also based on similar expansion of the forced response, the choice of Galerkin's orthogonalisation procedure to fulfil the continuity condition in a fluid and the selection of 'fluid-dominated' modes for this purpose appears to be physically more reasonable. Besides, unlike some previous research papers (e.g., Ref. [15]), the accuracy of such an approximate solution is consistently controlled (as is done in Ref. [6]) by the independent computations of acoustic and structural power transmission and checking the energy balance between them and the energy input.

Let M be the number of roots of the dispersion equation (15), which is used to construct Green's matrix. As is shown in Section 4, the dispersion equation (15) always has four roots, which satisfy all conditions at infinity in the case of no fluid loading. Apparently, $M > 4$ for a fluid-loaded shell. For example, if a lateral concentrated force is applied, a solution is formulated as

$$
\begin{aligned}
u_m^{03} &= \operatorname{sgn}(x-\xi)\sum_{j=1}^{M}\alpha_j C_j^{03}\exp\left(\frac{\tilde{k}_j}{R}|x-\xi|\right),\\
v_m^{03} &= \sum_{j=1}^{M}\beta_j C_j^{03}\exp\left(\frac{\tilde{k}_j}{R}|x-\xi|\right),\\
w_m^{03} &= \sum_{j=1}^{M} C_j^{03}\exp\left(\frac{\tilde{k}_j}{R}|x-\xi|\right),\\
\varphi_m^{03} &= \sum_{j=1}^{M} -\mathrm{i}\omega C_j^{03}\mathrm{I}_m(\kappa_j r)\left(\frac{\mathrm{d}\mathrm{I}_m(\kappa_j r)}{\mathrm{d}r}\bigg|_{r=R}\right)^{-1}\exp\left(\frac{\tilde{k}_j}{R}|x-\xi|\right).
\end{aligned}
\tag{22}
$$

The conditions at the loaded cross-section of a shell are still given by Eqs. (13). However, Eqs. (13) are not sufficient to uniquely define all unknown coefficients C_j^{03}, $j = 1, \ldots, M$. Their 'redundancy' is explained by the necessity to fulfil continuity conditions not only at the cross-section of a shell, but also in a fluid field at $x = \xi$. Due to the symmetry of this particular loading case, this condition is formulated as zero axial velocity

$$
\frac{\partial\varphi_m}{\partial\tilde{x}} = 0. \tag{23}
$$

If this equality holds exactly, then an exact formulation of Green's matrix is obtained. In practical computations, it is possible to retain in the series (22) only a finite number of terms. Then the Green's matrix is obtained approximately and the accuracy of its formulation may be assessed by the convergence rate of coefficients C_j^{03}, $j = 1, \ldots, M$ as the number M of terms increases.

In such an approximation, condition (23) is formulated in an averaged sense by the Galerkin method, and a system of equations defining coefficients C_j^{03}, $j = 1, \ldots, M$ is composed as

$$
\sum_{j=1}^{M}\alpha_j C_j^{03} = 0, \tag{24a}
$$

$$\sum_{j=1}^{M}\left[\frac{1-\nu}{2}+\frac{h^2}{12}\frac{2(1-\nu)}{R^2}\right]\beta_j\tilde{k}_j C_j^{03}=0, \tag{24b}$$

$$-\frac{h^2}{12R^2}\sum_{j=1}^{M}[\tilde{k}_j^3-(2-\nu)m\beta_j\tilde{k}_j]C_j^{03}=-\frac{1}{2}, \tag{24c}$$

$$\sum_{j=1}^{M}\tilde{k}_j C_j^{03}=0, \tag{24d}$$

$$\sum_{j=1}^{M}C_j^{03}\tilde{k}_j\left(\frac{\mathrm{d}\mathrm{I}_m(\kappa_j r)}{\mathrm{d}r}\bigg|_{r=R}\right)^{-1}\int_0^R \mathrm{I}_m(\kappa_j r)\mathrm{I}_m(\kappa_n r)r\,\mathrm{d}r=0,\ \ n=5,\ldots,M. \tag{24e}$$

In Eqs. (24), orthogonalisation is performed with the total velocity and the individual pressure distributions ($n=5,\ldots,M$) in the radial direction chosen as weight functions.

Condition (23) is applied to construct the row of Green's matrix for the loading of a shell by radial or circumferential forces concentrated in the axial direction. Here the deformation of the fluid-filled shell is symmetric with respect to a loaded cross-section and no fluid flow is admissible through this section, i.e., a 'rigid acoustic baffle' is inserted into the loaded cross-section. For a longitudinal loading, a set of 'skew-symmetric' conditions (10) should be supplemented by the condition $\varphi_m=0$ at $x=\xi$. This condition of a 'soft acoustic baffle' allows free penetration of fluid particles through the loaded section. Here orthogonalisation is performed with the total pressure against the individual velocity distributions ($n=5,\ldots,M$). Then a set of elements for the Green's matrix is obtained by solving this system of ($M\times M$) linear algebraic equations.

Conditions (24e) are formulated for a selected sub-set of roots ($n=5,\ldots,M$) from the dispersion equation (15). It may be advantageous to perform the orthogonalisation against fluid dominated roots. Potentially the roots originating from the introduction of fluid loading may here be distinguished from the original shell modes by gradually lowering the density $\rho_f\to 0$. However it is not always possible to perform a clear identification of 'shell originated' and 'fluid originated waves'. A complex conjugate wave in the fluid-loaded shell may develop from two decaying waves, one originating from the shell and the other originating from the fluid. In order to indicate the stability of the approximation, calculations were performed with different number of roots (M) and with orthogonalisation against different sub-sets ($n=5,\ldots,M$). From this investigation a fine stability on the power flow was found even with a limited number of roots included.

9. Dispersion curves—including internal fluid loading

In Fig. 13 dispersion curves are plotted for the cylindrical shell introduced in Section 5, but now filled with an acoustic medium of $\rho_f=1000\ \mathrm{kg/m^3}$ and $c_f=1440\ \mathrm{m/s}$. Again a zoom is performed in the regions of cut-on and from Fig. 14 it is seen that bifurcation phenomena similar to those found for the shell without fluid appear. It is noted that the first cut-on now takes place at 928 Hz as compared with 1659 Hz for the shell without fluid—a significant drop due to the rather small thickness of the shell. A second cut-on appears at 64 kHz and a third around 77 kHz. Or

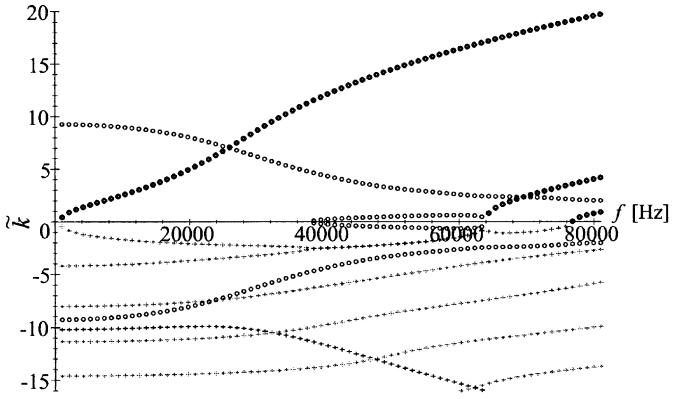

Fig. 13. Dispersion for shell with fluid, $m = 3$: + Comp, Re; ◦ Comp, Im; + Decay; • Prop.

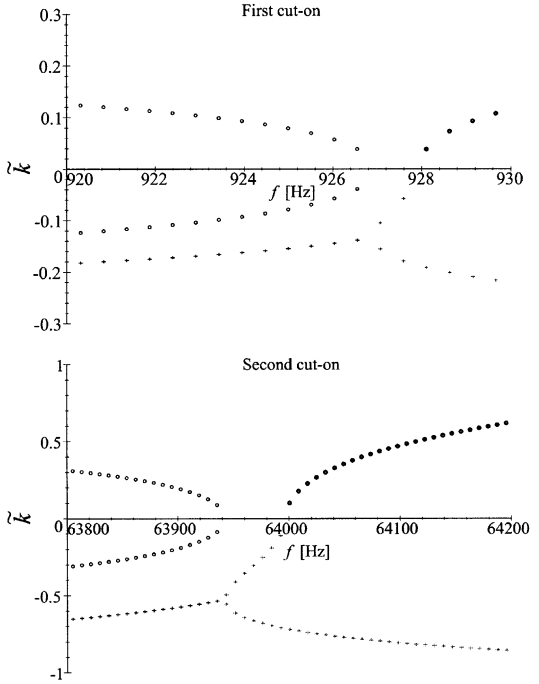

Fig. 14. Bifurcation at first and second cut-on for shell with fluid, $m = 3$: + Comp, Re; ◦ Comp, Im; + Decay; • Prop.

rather at 76822.2 Hz, exactly the same frequency as the second cut-on appeared for the shell without fluid. This is clearly seen from the modal coefficient α_3 for the shell without fluid that peaks at this specific frequency. This means there is no coupling between u and w and for a finite value of u there will be no w displacement and thus no coupling to the fluid for this wave at this specific frequency.

10. Power flow—including internal fluid loading

The presence of fluid loading does not modify the formulation of power flow of structural waves (18). However, due to the compressibility of the fluid some amount of energy may 'escape' from a structural path and be transported through the fluid. The formulation of the energy transported through the acoustic medium is

$$N^{fluid}_{m,out} = -\gamma \frac{\pi\omega}{2} \int_0^R [\mathrm{Im}(p_m)\,\mathrm{Re}(u_{fl,m}) - \mathrm{Re}(p_m)\,\mathrm{Im}(u_{fl,m})] r\,\mathrm{d}r, \tag{25}$$

where $u_{fl,m}$ is the longitudinal displacement in the fluid.

An energy conservation law may then be formulated as

$$N^{tot}_{m,out} = N^{axial}_{m,out} + N^{torsion}_{m,out} + N^{bending}_{m,out} + N^{fluid}_{m,out}. \tag{26}$$

As follows from this equation, the mechanical energy injected is spread over four paths—a very important fact from a practical point of view. In many cases, this phenomenon may be undesirable because it makes mechanical suppression of vibrations at the surface of the shell inefficient in avoiding energy transportation to the far field.

In Fig. 15 the power flow is displayed for low frequency excitation at 2000 Hz, where only one wave may propagate. To the left is displayed the structural power flow in the same way as for the shell without fluid and to the right a comparison between the calculated gain in fluid power N^{fluid} and the loss of structural power $-\Delta N^{str,0}$ as referred to the cross-section of excitation. It is noted that the structural power flow has resemblance to the energy distribution in Fig. 15 for excitation at 4000 Hz for a shell without fluid. Actually the wave propagating at 2000 Hz for the shell with fluid is almost identical to the wave propagating in the shell without fluid at 3500 Hz. At 2000 Hz the shell with fluid has $k = 0.872$, $\alpha = 0.080$ and $\beta = -0.339$ versus $k = 0.867$, $\alpha = 0.080$ and $\beta = -0.339$ at 3500 Hz for the shell with fluid. At the low frequencies only a very small amount of energy—in this case 1.4%—is carried in the fluid. The fluid primarily acts as 'added mass' in the low-frequency range.

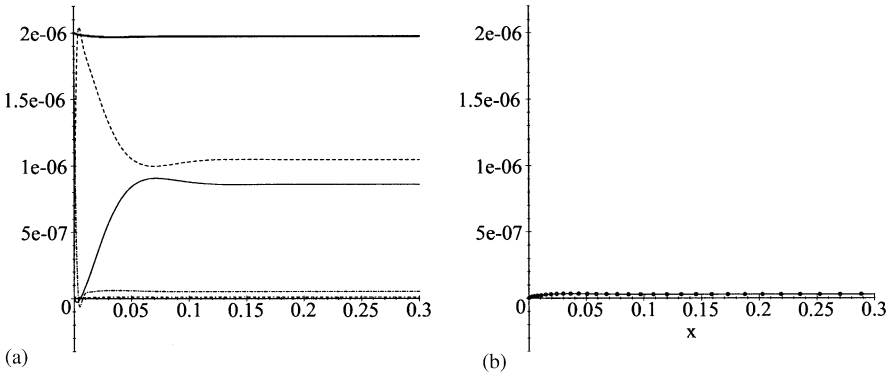

Fig. 15. Power flow in structure and fluid for radial excitation, $f = 2000$ Hz, $m = 3$: (a) —— N^{axial}; ---- $N^{torsion}$; –○–○– $N^{bending,w}$; ○○–○○–○○ $N^{bending,w'}$; —— $N^{scr,tot}$; (b) ○ N^{fluid}; —— $-\Delta N^{str,0}$.

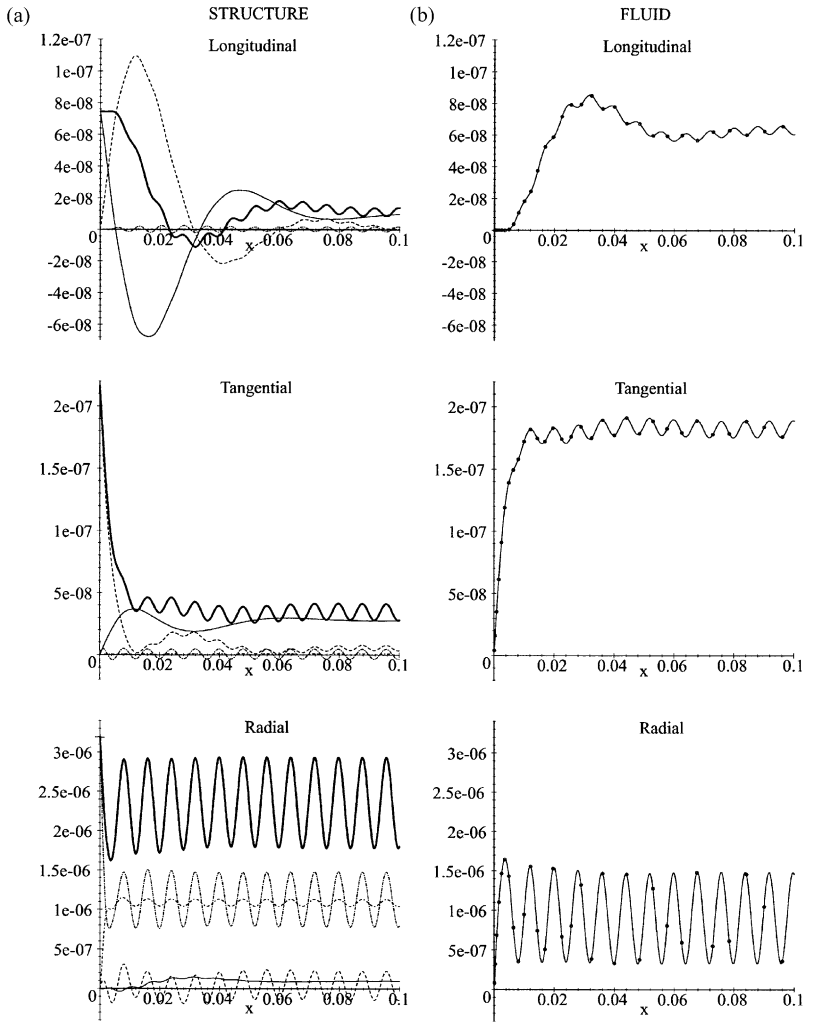

Fig. 16. Power flow in structure and fluid for longitudinal, tangential and radial excitation, $f = 68$ kHz, $m = 3$: (a) —— N^{axial}; ---- $N^{torsion}$; –○–○– $N^{bending,w}$; ○○–○○–○○ $N^{bending,w'}$; —— $N^{scr,tot}$; (b) ○ N^{fluid}; —— $\Delta N^{str,0}$.

At higher frequencies an increasing amount of the power flow may take place in the fluid. Then steady spatial fluctuation of the energy between structural and acoustic transmission paths are observed. The ratio of power in the fluid to the total power and the amount of oscillation will depend very much upon the excitation conditions as shown in Fig. 16. Here the power flow is shown for an excitation frequency of 68 kHz and $m = 3$. The wave cut-on firstly would carry only 10% of its energy in the fluid whereas the wave cut-on secondly would carry almost 85% if excited alone. Thus the final power flow balance will again depend significantly upon magnitude and phase of the two waves. For all three loading cases a very fine agreement is found between the calculated loss in structural power and the gain in fluid power as is seen in the right hand side of Fig. 16.

11. Conclusions

This paper presents a consistent derivation of the boundary integral method for cylindrical shells with fluid loading together with a thorough discussion of its versatile application. It is illustrated how the method allows detailed studies to be performed on finite as well as infinite structures and how it handles 'light' as well as 'heavy' fluid loading. Furthermore the method makes it possible to handle nearfield and farfield analysis within the same analytic tool and provides profound insight into the complex energy redistribution in the zone of transition.

Within a homogeneous problem formulation, typical dispersion curves are presented and phenomena of bifurcations and cut-on are studied. It is also illustrated how modal coefficients may bring valuable information for interpretation of the dynamic behaviour. As is shown in the paper, the energy distribution between various wave numbers and various transmission paths in a shell of given parameters is very sensitive to the excitation frequency. Also, the energy distribution between axial, torsional, flexural and acoustical components in the far field may be very different from those in the near field. Moreover in cases when a shell supports more than one propagating wave, steady fluctuations between these components are strongly affected by the excitation conditions. All these features are adequately captured by the boundary equations method which is also applicable for analysis of finite structures. For the finite cylindrical shell the boundary integral method has been compared with traditional finite element analysis in terms of eigenfrequencies, and excellent agreement has been found.

The work has also highlighted the potential of the boundary integral approach in analysis of more complicated problems in dynamics of fluid–structure coupled systems. It particular, formulation of Green's matrices makes it possible to introduce a concept of sub-structuring to describe wave propagation and power flow in complex systems. Furthermore, the explicit formulation of Green's functions offers numerous possibilities of averaging in the frequency domain as well as in the spatial domain. This means the boundary integral method may also supply input for statistical energy based analysis procedures in the high frequency domain, one of the strengths here being the consistent transition from deterministic, displacement based analysis to a statistical and energy-based approach.

Appendix. The shell theory used: sign convention and formulas for deformations and force resultants

The positive directions of the displacements and driving forces are shown in Fig. 17. Within the framework of Gol'denveiser–Novozhilov theory [17,18] the components of mid-plane deformation are

$$\varepsilon_1 = \frac{\partial u}{\partial x} \text{ (the deformation in the axial direction)},$$

$$\varepsilon_2 = \frac{1}{R}\frac{\partial v}{\partial \theta} + \frac{w}{R} \text{ (the deformation in the circumferential direction)},$$

$$\varpi = \frac{1}{R}\frac{\partial u}{\partial \theta} + \frac{\partial v}{\partial x} \text{ (the shear deformation)},$$

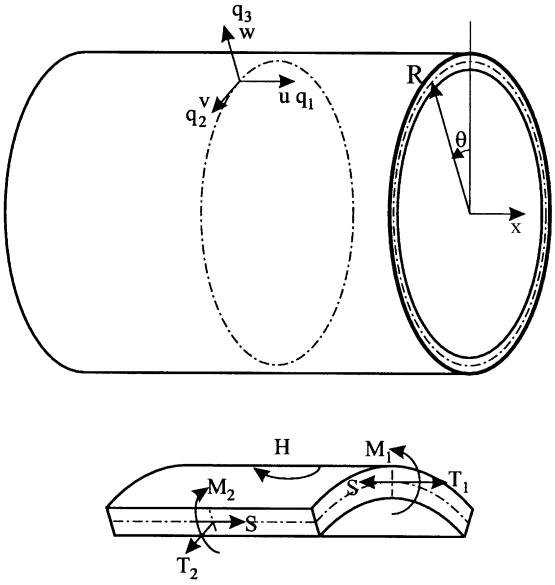

Fig. 17. The sign convention in the shell theory.

$$\kappa_1 = -\frac{\partial^2 w}{\partial x^2} \text{ (the bending curvature in the axial direction)},$$

$$\kappa_2 = -\frac{1}{R^2}\frac{\partial^2 w}{\partial \theta^2} + \frac{1}{R^2}\frac{\partial v}{\partial \theta} \text{ (the bending curvature in the circumferential direction)},$$

$$\tau = -\frac{1}{R}\frac{\partial^2 w}{\partial x\,\partial \theta} + \frac{1}{R}\frac{\partial v}{\partial x} \text{ (the twisting)}.$$

Force and moment resultants in a shell element are, respectively [17,18],

$$T_1 = \frac{Eh}{1-\nu^2}\left(\frac{\partial u}{\partial x} + \frac{\nu}{R}\frac{\partial v}{\partial \theta} + \frac{\nu}{R}w\right) \text{ (the axial membrane force)},$$

$$T_2 = \frac{Eh}{1-\nu^2}\left(\nu\frac{\partial u}{\partial x} + \frac{1}{R}\frac{\partial v}{\partial \theta} + \frac{1}{R}w\right) \text{ (the circumferential membrane force)},$$

$$S = \frac{Eh}{1-\nu^2}\frac{1-\nu}{2}\left(\frac{\partial v}{\partial x} + \frac{1}{R}\frac{\partial u}{\partial \theta}\right) \text{ (the shear force)},$$

$$M_1 = \frac{Eh^3}{12(1-\nu^2)}\left(-\frac{\partial^2 w}{\partial x^2} - \frac{\nu}{R^2}\frac{\partial^2 w}{\partial \theta^2} + \frac{\nu}{R}v\right) \text{ (the axial bending moment)},$$

$$M_2 = \frac{Eh^3}{12(1-\nu^2)}\left(-\nu\frac{\partial^2 w}{\partial x^2} - \frac{1}{R^2}\frac{\partial^2 w}{\partial \theta^2} + \frac{1}{R}\nu\right) \text{(the circumferential bending moment)},$$

$$H = \frac{Eh^3}{12(1-\nu^2)}(1-\nu)\left(-\frac{1}{R}\frac{\partial^2 w}{\partial x \partial \theta} + \frac{1}{R}\frac{\partial v}{\partial x}\right) \text{ (the twisting moment)}.$$

They are also shown in Fig. 17.

References

[1] M. Junger, D. Feit, *Sound, Structures and their Interaction*, MIT Press, Cambridge, MA, 1993.
[2] C.R. Fuller, S.J. Elliot, P.A. Nelson, *Active Control of Vibration*, Academic Press, London, 1995.
[3] S.V. Sorokin, Boundary integral equations method in dynamics of complex thin-walled structures, *Transactions of Gor'kij State University* 24 (1990) 64–75 (in Russian).
[4] S.V. Sorokin, Analysis of structural-acoustic coupling problems by a two-level boundary integral equations method. Part 2. Vibration of a cylindrical shell of a finite length in an acoustic medium, *Journal of Sound and Vibration* 184 (2) (1995) 213–228.
[5] S.V. Sorokin, Vibrations of and sound radiation from sandwich plates in heavy fluid loading conditions, *International Journal of Composite Structures* 48 (2000) 219–230.
[6] S.V. Sorokin, Analysis of vibrations and energy flows in sandwich plates bearing concentrated masses and spring-like inclusions in heavy fluid loading conditions, *Journal of Sound and Vibration* 253 (2) (2002) 485–505.
[7] C. Durant, G. Robert, P.J.T. Filippi, P.-O. Mattei, Vibro-acoustic response of a thin cylindrical shell excited by a turbulent internal flow: comparison between numerical prediction and experimentation, *Journal of Sound and Vibration* 229 (5) (2000) 1115–1155.
[8] R.S. Ming, J. Pan, M.P. Norton, The mobility functions and their application in calculating power flow in coupled cylindrical shells, *Journal of Acoustical Society of America* 105 (3) (1999) 1702–1713.
[9] S.V. Sorokin, J. Balle Nielsen, N. Olhoff, Analysis and optimisation of energy flows in structures composed of beam elements—Part I: problem formulation and solution technique, *Journal of Structural Optimization* 22 (2001) 3–11.
[10] C.R. Fuller, F.J. Fahy, Characteristics of wave propagation and energy distributions in cylindrical shells filled with fluid, *Journal of Sound and Vibration* 81 (4) (1982) 501–518.
[11] C.R. Fuller, The input mobility of an infinite circular cylindrical shell filled with fluid, *Journal of Sound and Vibration* 87 (3) (1983) 409–427.
[12] G. Pavic, Vibrational energy flow in elastic circular cylindrical shells, *Journal of Sound and Vibration* 142 (2) (1990) 293–310.
[13] G. Pavic, Vibroacoustical energy flow through straight pipes, *Journal of Sound and Vibration* 154 (3) (1992) 411–429.
[14] L. Feng, Acoustic properties of fluid-filled elastic pipes, *Journal of Sound and Vibration* 176 (3) (1994) 399–413.
[15] M.B. Xu, W.H. Zhang, Vibrational power flow input and transmission in a circular cylindrical shell filled with fluid, *Journal of Sound and Vibration* 234 (3) (2000) 387–403.
[16] O. Fegeant, Closed from solutions for the point mobilities of axisymmetrically excited cylindrical shells, *Journal of Sound and Vibration* 243 (1) (2001) 89–115.
[17] A.W. Leissa, *Vibrations of Shells*, NASA SP-288, 1973.
[18] A.L. Gol'denveiser, V.B. Lidskij, P.E. Tovstik, *Free Vibrations of Thin Elastic Shells*, Nauka, Moscow, 1979 (in Russian).
[19] V.V. Novozhilov, *Theory of Thin Shells*, Sudostroenie, Leningrad, 1962 (in Russian).